

RESEARCH

Open Access



# Evaluation on the Bond Capacity of the Fire-Protected FRP Bonded to Concrete Under High Temperature

Soo-yeon Seo<sup>1\*</sup> , Jong-wook Lim<sup>2</sup> and Su-hyun Jeong<sup>1</sup>

## Abstract

To figure out the change in the reinforcing effect of FRP system used for the retrofit of RC beam when it is exposed to high temperature, it is required to evaluate not only the behavior of the entire beam, but also the bond performance at anchorage zone through a bond test according to the increase of external temperature. Moreover, the study to find various fire-protection methods is necessary to prevent the epoxy from reaching the critical temperature during an exposure to high temperature. In this manner, the fire-resistance performances of externally bonded (EB) FRP and near-surface-mounted (NSM) FRP to concrete block were evaluated by high-temperature exposure tests after performing a fire-protection on the surface in this paper. Board-type insulation with mortar was considered for the fire-protection of FRP system. After the fire-protection of the FRPs bonded to concrete blocks, an increasing exposure temperature was applied to the specimens with keeping a constant shear bond stress between concrete and the FRP. Based on the result, the temperature when the bond strength of the FRP disappears was evaluated. In addition, a finite element analysis was performed to find a proper method for predicting the temperature variation of the epoxy which is fire-protected with board-type insulation during the increase of external temperature. As a result of the test, despite the same fire-protection, NSM specimens were able to resist 1.54–2.08 times higher temperature than EB specimens. In the design of fire-protection of FRP system with the board-type insulation, it is necessary to consider the transfer from sides as well as the face with FRP. If there is no insulation of FP boards on the sides, the epoxy easily reaches its critical temperature by the heat penetrated to the sides, and increasing the thickness of the FP board alone for the face with FRP does not increase the fire-resistance capacity. As a result of the FE analysis, the temperature variation at epoxy can be predicted using the analytical approach with the proper thermal properties of FP mortar and board.

**Keywords:** bond performance, anchorage zone, externally bonded (EB) FRP, near-surface-mounted (NSM) FRP, fire-protection, board-type insulation with mortar, finite element analysis

## 1 Introduction

In the strengthening of Reinforced Concrete (RC) structure, a method of using Fiber Reinforced Polymer (FRP) has been widely used since it has high strength with light weight and excellent workability (ACI 440.2R 2008; Fib

TG9.3 2001). FRPs may consist of carbon, glass, aramid and basalt fibers that are bonded together by the matrix of a polymer such as epoxy, vinyl ester or polyester to form CFRP, GFRP, AFRP and BFRP, respectively (Teng et al. 2003; Hollaway 2011; Sidduka et al. 2020; ACI 440.2R 2008; Fib TG9.3 2001). FRP materials have been used in the forms of laminates, rods, dry fibers or sheets in concrete structures (ACI 440.2R 2008; Fib TG9.3 2001; Sidduka et al. 2020). Strengthening methods for RC member are classified into Externally Bonded (EB) Retrofit and Near-Surface-Mounted (NSM) Retrofit. In EB method,

\*Correspondence: syseo@ut.ac.kr

<sup>1</sup> School of Architecture, Korea National University of Transportation, Chungju, South Korea

Full list of author information is available at the end of the article

Journal information: ISSN 1976-0485 / eISSN 2234-1315

FRP is attached to the surface of a concrete member using epoxy resin. This method is relatively excellent in workability, but it requires a surface treatment process of concrete for a perfect bonding of FRP. Since the FRP bonded to concrete is exposed to the external environment, an adhesion failure of it is likely to occur unless the surface is suitably protected. NSM method, on the other hand, requires additional processing by forming a groove in the concrete member and then embedding the FRP in it, but does not require any surface treatment work and has relatively excellent adhesion performance (Sena Cruz and Barros 2004; Lorenzis et al. 2004; Teng et al. 2006; Seracino et al. 2007; Al-Mahmoud et al. 2012; Seo et al. 2013, 2016a,b).

About thermal capacity of FRP system, the glass transition temperature  $T_g$  of FRP, which is called as a critical temperature, is typically in the range of 93–120 °C (ACI 440.1R 2015) and that of epoxy resin for attaching FRP reinforcement is 60–82 °C for existing, commercially available FRP system (ACI 440.2R 2008). Therefore, when the concrete structure reinforced with FRP exposed to a high temperature such as a fire, the epoxy around FRP reinforcement easily reaches its  $T_g$  even at low temperature, and the adhesion capacity is disappeared. (Blontrock et al. 1999; Kodur et al. 2007; Wang et al. 2007; Foster and Bisby 2008; Nigro et al. 2011a, b, 2012; Katz et al. 1999). In consideration of such conditions, the strength of FRP for design purpose is to be ignored unless a fire-protection system can maintain the FRP temperature below its critical temperature (ACI 440.2R 2008; Fib TG9.3 2001). In this respect, a series of studies have been conducted to ensure the fire-resistance performance of the RC member reinforced with FRP (Blontrock et al. 2001; Bisby et al. 2005; Burke et al. 2013; Foster and Bisby 2008; Williams et al. 2008; Chowdhury et al. 2008; Kodur and Ahmed 2010; Hajiloo et al. 2017).

Foster and Bisby (2008) performed an analysis of the several test results (such as tension coupon tests, single-lap FRP-to-FRP bond tests, direct tension FRP-to-concrete bond tests, and pull-apart FRP-to-concrete shear bond tests) after exposure to temperatures up to 400 °C. As a result, they revealed that the residual properties of externally bonded FRP systems after high-temperature exposure appear to be influenced predominantly by the properties of the resin system used for the adhesion of the FRP; the fiber type does not appear to influence residual performance. From the test to find the change of the bond performance of epoxy in NSM retrofit with temperature, Palmieri et al. (2011) found that the bond performance of NSM-FRP bars decreased considerably at the  $T_g$  of epoxy, 65 °C and the bars were separated from the concrete due to the interface failure at 100 °C. From additional test, Palmieri (2012) found that the properly

insulated NSM-FRP strengthened in beams can achieve a fire endurance of at least 2 h. In addition, from the tests of the beams exposed to 1 h of fire, Palmieri et al. (2013) suggested that if the insulation system is able to maintain the adhesive temperature at a relatively low value (not larger than 160% of  $T_g$  of epoxy), the bond degradation of FRP under fire is limited, and the beam strengthened with FRP can retain a large part (up to 92%) of its original strength. From a fire loading test on an RC beam strengthened with carbon FRP (CFRP), also Ahmed and Kodur (2010) found that the anchorage configuration plays a critical role in limiting the deflections of the strengthened beam after debonding of the FRP occurs at around  $T_g$  of epoxy. Furthermore, FRP-strengthened RC beams supplemented with 25-mm-thick spray-applied insulation can survive failure under ASTM E119 (2007) standard fire or a design fire. Seo and Kim (2013) carried out tensile tests of CFRP plates, epoxy state change tests, and bond performance tests under increasing temperature conditions. The research found that the NSM retrofit is an effective reinforcing method in terms of bond strength but the reinforcing effect may be considerably reduced as the surrounding temperature goes up. Specifically, it found that the bond function of epoxy is lost when the surrounding temperature approaches the  $T_g$ , 65 °C, at which the chemical characteristics of epoxy begin to change. Jiangtao et al. (2017) reported that  $T_g$  may be over-conservative as the critical temperature to determine the fire resistance of the NSM-CFRP strengthening system through a fire loading test of RC beam strengthened with NSM-CFRP.

In addition to experimental researches, numerical procedures have been performed to simulate the thermomechanical response of RC member strengthened with FRPs under exposure to fire. Kodur and Ahmed (2010) presented numerical procedures capable of simulating the thermomechanical response of RC beams strengthened with EB-CFRP strips under exposure to fire. In the models, the temperature-dependent material properties of FRP and adhesive were considered and after performing a 2D heat transfer analysis of the cross section, they use moment–curvature relationships to trace the mechanical response of the beams. In these two researches, the difference is that the bond degradation at the CFRP–concrete interface, particularly the bond-slip as a function of temperature is explicitly simulated in latter. As extended research, Kodur and Yu (2013) suggested an approach to trace the response of NSM-FRP-strengthened RC beam from the preloading stage to collapse under a specified fire exposure and loading conditions. The model accounts for high-temperature properties of constitutive materials, realistic load and boundary conditions, and temperature-induced bond degradation at the FRP–concrete interface.

Kodur and Bhatt (2018) applied this analytical approach to evaluate the performance of FRP-strengthened RC slab under fire conditions.

About the insulated FRP reinforcing system, Dai et al. (2015) developed 3D finite element model considering the bond degradation with temperature of both internal steel and external FRP reinforcement to simulate the thermal and structural behavior of insulated EB-FRP-strengthened RC beams exposed to fire. Firmo et al. (2015) simulated the thermomechanical response of EB-CFRP-strengthened beams subjected to fire and protected with different insulations. Two-dimensional (2D) FE models of the beams were developed using a commercial software, where the CFRP–concrete interaction was modeled by means of bi-linear bond-slip laws previously calibrated up to 120 °C. As extended research, Frimo et al. (2018) performed 3D-FE analysis to simulate the fire behavior of RC beams flexurally strengthened with NSM-CFRP techniques. From these two researches, they confirmed that the thermal response of the insulated CFRP-strengthened RC beams subjected to fire, in particular the temperature distribution along the EB-CFRP–concrete and NSM-CFRP–concrete interfaces could be accurately simulated.

These previous researches present that the bond performance of FRP bonded to concrete will be reduced if the FRP is exposed to a high temperature. The temperature at which the bond strength decreases is closely related to the  $T_g$  of epoxy, but its limit is still unclear. In particular, according to the previous research results, in the case of beams reinforced with FRP, it was found that the adhesion performance of the epoxy was maintained in the range of 1.0–1.6 times  $T_g$ . This performance seems to be due to the fact that the end fixing performance of the FRP is properly kept even when exposed to high temperatures. Therefore, to figure out the change in the bond performance of FRP according to the temperature increase, not only the behavior of the entire beam, but also the performance evaluation is required on the anchorage zone according to the external temperature. Moreover, it is required to study various reinforcing technologies for a proper fire-insulation to prevent the epoxy from reaching the limit temperature and maintain a sufficiently low temperature.

Accordingly, this study aims to evaluate the fire-resistance performance of FRPs reinforced to concrete subjected to increasing temperature under constant bond stress. Two types of retrofits, EB and NSM methods are considered in the test plan and board-type insulators with mortar are used for fire-protection. After keeping constant load at the end of FRP to act a bond stress at the interface between FRP and concrete, the increasing exposure temperature is applied to FRP surface with various

details of the insulation for fire-protection to determine the temperature at which the FRP loses its bond strength. In addition, a finite element analysis is performed to find a proper method for predicting the temperature variation of the epoxy which is fire-protected with board-type insulation during external temperature increase.

## 2 Evaluation on the Bond Capacity of Fire-Protected FRP Bonded to Concrete at High Temperature

### 2.1 Design of Specimen

To evaluate the performance of the FRP bonded to concrete members under high temperature, a bond test is planned. The variables of the experiment are the reinforcement method of FRP, the thickness of fireproof insulation and the number of insulated surfaces. The strengthening methods using FRP reinforcement considered in this study are EB and NSM. The shape of the specimens and the concept of fire-protection are shown in Fig. 1. The list of specimens is shown in Table 1.

Eight 100 mm × 100 mm × 200 mm size concrete blocks were made. In making an EB specimen, epoxy was pre-applied to the front surface of four concrete blocks, and then carbon FRP with a thickness of 1.2 mm and a width of 34 mm was attached. For NSM specimens, a groove of 5 mm wide and 20 mm deep is formed in each concrete block over its entire length and CFRP having a thickness of 1.2 mm and a width of 17 mm was embedded in the groove. Regarding this groove, ACI 440.2R (2008) recommends a width of at least 3.0 times the thickness of the FRP and 1.5 times the width of the FRP for rectangular FRP reinforcement in NSM system. The width of the groove in the specimens is 3.6 mm, which satisfies the condition, but the depth is 25.5 mm which is somewhat insufficient. However, as a result of using a groove of this shape in the previous experiments (Seo et al. 2013, 2016a,b), a sufficient adhesion strength was exhibited, so the same shape of the groove was also set in this experiment.

For each EB and NSM-FRP systems, two cases of fire-protection were considered such as the case where only the front surface is fire-protected by the board with mortar and the case where the front and sides are fire-protected. The insulation thickness of 25 mm or 45 mm are planned for the front face with FRP while 15 mm for both sides.

The cross-sectional area of FRP is doubled in EB specimen compared to NSM specimen, but the adhesion area is the same. In both cases, the bond length is 100 mm so that bond failure dominates the overall behavior. For side insulations, the fire-protection (FP) boards were attached to only 75 mm of 100-mm depth

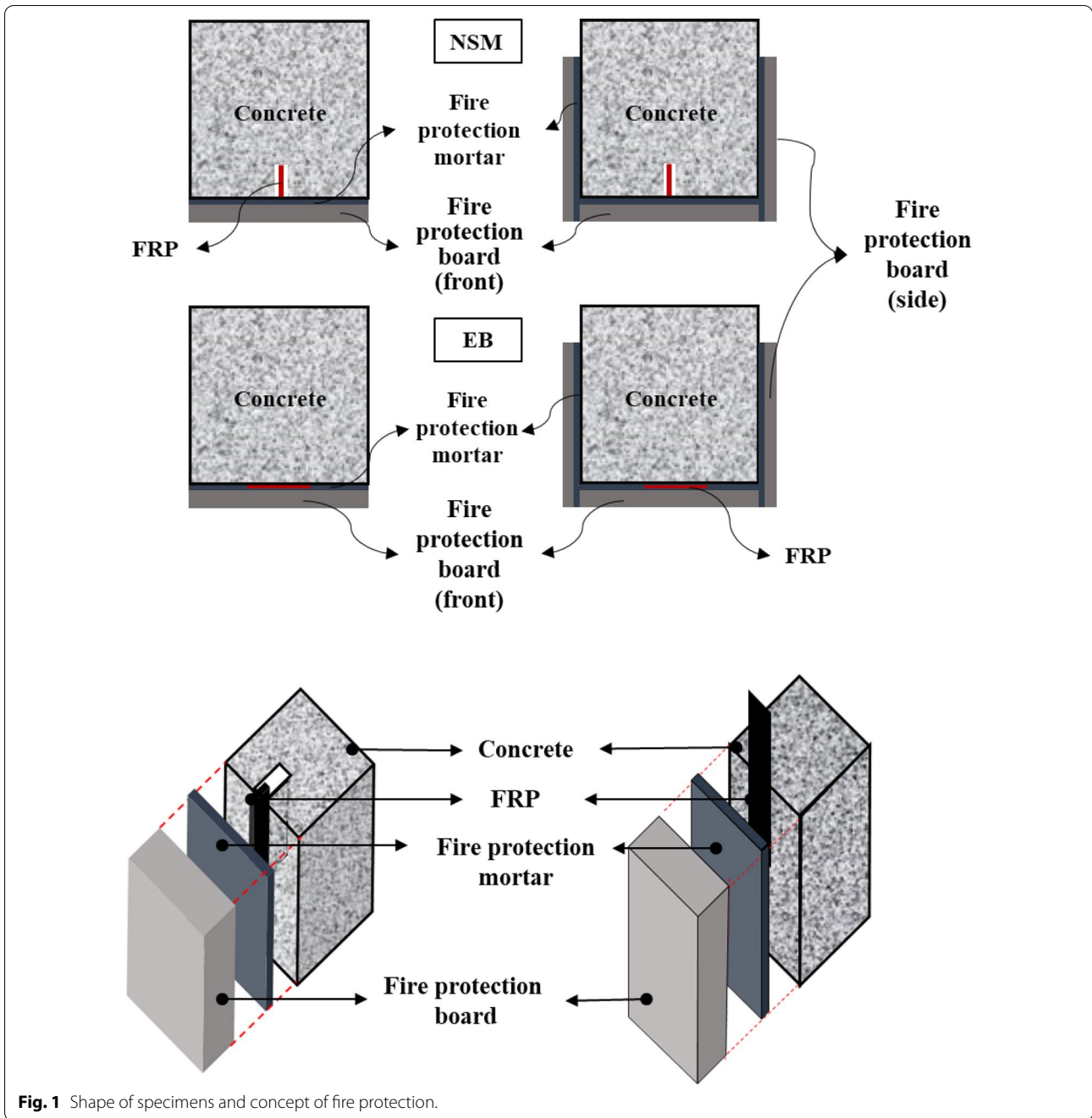


**Fig. 1** Shape of specimens and concept of fire protection.

of block. Therefore, the remaining 25 mm was allowed to be exposed. Figure 2 shows the dimensions of the specimens reinforced with EB and NSM.

To measure the temperature of the epoxy in the specimens during the experiment, the thermocouples were installed as shown in Fig. 2, and then the FP board was attached to the surface using fire protection mortar (FP mortar). Figure 3 shows the appearance after reinforcing fire protection for NSM specimen. In case of EB

specimens, the method of fire protection is same as that of NSM specimen.

**2.2 Material Properties**

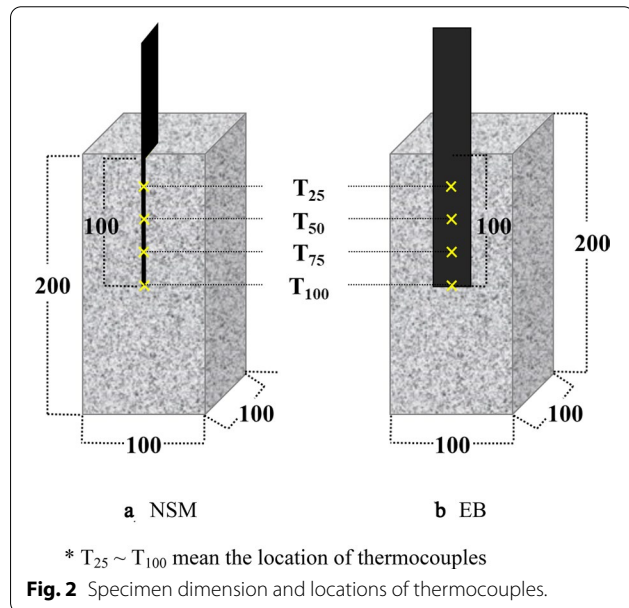
The 28-day compressive strength of the concrete block was 21 MPa. SK-CPS0512 and SK-CPA10 were used for the CFRP strip and epoxy, respectively. The tensile strength and modulus of elasticity of CFRP provided by the manufacturer are 2942 MPa and 165,000 MPa,

**Table 1 Specimen list.**

Specimen name <sup>a</sup>	Strengthening method	Fire protection	Thickness of insulator (mm)		Stress acting on FRP <sup>b</sup>
			Front	Sides	
E-F0-S0	Externally bonded	None	None	None	Increase up to failure $0.4P_{n-E}$
E-F25-S0		Front	25	None	
E-F45-S0			45	None	
E-F25-S15		Front and sides	25	15	
E-F45-S15			45	15	
N-F0-S0	Near-Surface-Mounted	None	None	None	Increase up to failure $0.4P_{n-N}$
N-F25-S0		Front	25	None	
N-F45-S0			45	None	
N-F25-S15		Front and sides	25	15	
N-F45-S15			45	15	

<sup>a</sup> E Externally bonded, N near surfaced mounted, F front insulation, S side insulation.

<sup>b</sup>  $P_{n-E}$  and  $P_{n-N}$ : Bond strengths achieved from the tensile test of E-F0-S0 and N-F0-S0 without exposure to high temperature, respectively.



respectively. The actual tensile strength and modulus of elasticity of the CFRP obtained from tensile tests in this study are 2319 MPa and 222,851 MPa, respectively. The strength properties of the epoxy are shown in Table 2. Glass Transition Temperature,  $T_g$  of a material can be found through the Differential Scanning Calorimetry (DSC) test. DSC is the most frequently used thermal analysis technique. It measures enthalpy changes in samples due to changes in their physical and chemical properties as a function of temperature or time. Three specimens of CFRP and epoxy were prepared each and subjected to DSC test using the test equipment as shown in Fig. 4. As a result, the average  $T_g$  of epoxy was 54.5 °C, and the decomposition temperature of FRP was

**Table 2 Strength properties of epoxy.**

	Strength (N/mm <sup>2</sup> ) <sup>a</sup>	Test method
Compressive strength	More than 90	ASTM D 695
Tensile shear bond strength	More than 10	ASTM D 1002
Bond strength to concrete	More than 1.5	JIS K 5400

<sup>a</sup> The values are given by manufacturers.

231.09 °C. The adhesion performance of FRP reinforced to concrete is greatly influenced by the performance of epoxy. In particular, when exposed to high temperatures, the adhesion capacity of the epoxy may be lost first. A bond-shear experiment of epoxy was performed to check



**Fig. 4** DSC test equipment.

the critical temperature at which the bond strength of reinforced FRP disappears. Three double shear specimens were made and tested as shown in Fig. 5. It will ascertain the critical temperature at which the bond strength of the epoxy is lost by causing certain level of shear stress to the epoxy and then exposing it to gradually increasing temperatures. Using epoxy, W 20 mm × H 5 mm steel plates were attached to each other with a length of 50 mm to have double shear surfaces. The specimens were installed for the epoxy bonding surface to be positioned inside the heating furnace, while the upper and lower ends of the FRP penetrate the holes located at the upper and lower sides of the heating furnace and are fastened to the UTM (Universal Testing Machine) jigs. After fixing both ends of the specimen securely to the grip, a stress equivalent to 40% of expected ultimate shear strength of epoxy was applied. The inside temperature of the heating furnace was gradually increased according to the planned heating curve until bond failure occurred while keeping the stress constant. The temperature was measured at the top and bottom of the epoxy ( $T_1$  and  $T_2$  in Fig. 5). Figure 6 shows the test results with a graph, where (a) is the temperature of epoxy of three specimens as the average value of  $T_1$  and  $T_2$  of the three specimens. (b) shows the change of the applied load (8kN) during the temperature change. The shear stress acting on the bond surface of epoxy was lost when the epoxy temperature reaches about 60 °C (54.4–60.5 °C). From this, it can be seen that the epoxy loses its adhesion at around 60 °C which is similar to 54.5 °C obtained from DSC.

The material properties of FP mortar for bonding FP board to the reinforced FRP are shown in Table 3. The characteristics FP board are shown in Table 4. These are all commercial products and their material properties are provided by manufacturers.

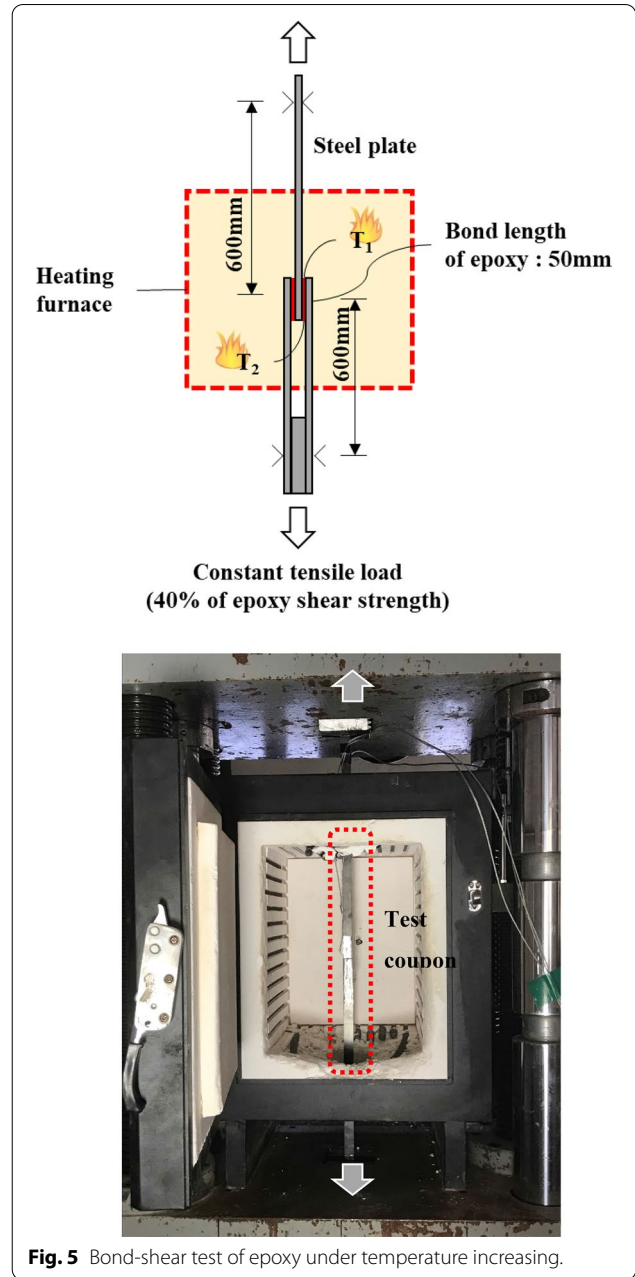
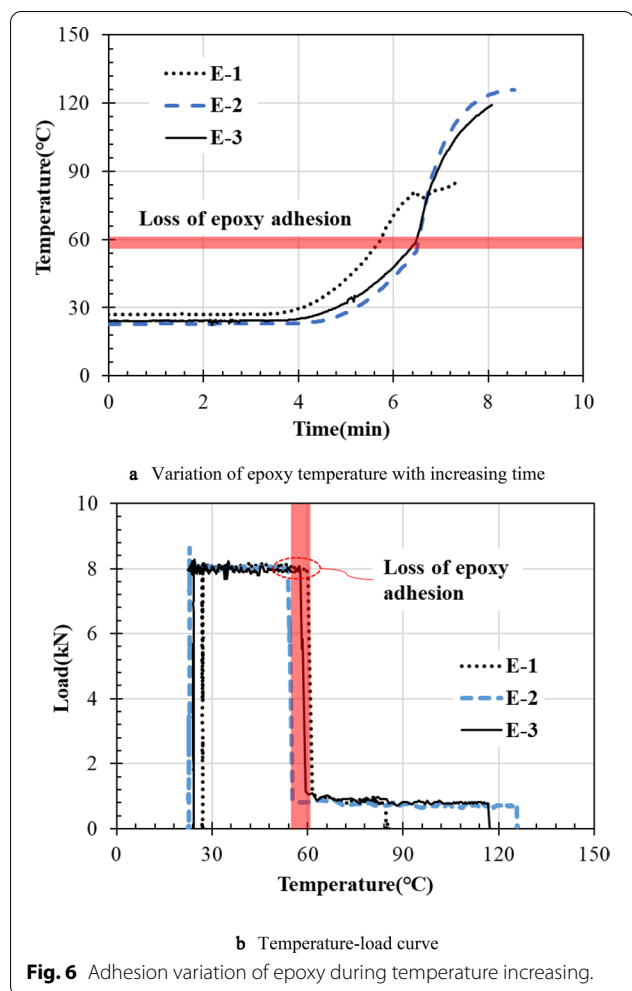


**Fig. 5** Bond-shear test of epoxy under temperature increasing.

The board thickness used for this study is 15 mm, 25 mm and 45 mm. To investigate the thermal conductivity of FP mortar and FP board, direct thermal conductivity test was performed in Korea Conformity Laboratories for each of the three specimens. As a result, the average thermal conductivity of FP mortar and FP board was 0.41 and 0.063 W/mK, respectively.



### 2.3 Measurement and Test Method

Thermocouples were installed to measure temperature changes in the furnace and in the epoxy used for bonding FRP to concrete. After reinforcing the concrete block with FRP, the thermocouples were spaced 25 mm between 25 and 100 mm from the end of the specimen in the direction of force, as shown in Fig. 2. The thermocouples were positioned in the epoxy between the FRP and the concrete for the EB specimens. In NSM specimens, thermocouples were placed in a central position in the depth direction of the FRP strip. To apply the tensile force, two steel plates with 100-mm length were reinforced with epoxy on both sides of the loading end of the FRP. Also, to prevent damage during the high-temperature exposure of FRP exposed to the upper part inside the furnace, as shown in Fig. 7, the FRP is protected in the shape of '□' with FRP board. After placing the specimen inside the heating furnace, the FRP protruding from the upper part was fixed to the biting device of the universal testing machine, and the concrete block was fixed to the lower part of the device for fixing the block. Figure 8 represents the specimen installed inside the furnace.

Two experiments, (1) increasing ultimately the tensile force until failure without exposing to high temperature and (2) increasing the temperature load while applying a predetermined stress and keeping it constant, were conducted. First, for the E-F0-S0 and N-F0-S0 specimens, the tensile strength was gradually increased until the final fracture to determine the maximum strength and the sliding displacement at this time under room temperature. For the specimens with fire-protection, the temperature was gradually increased until the adhesion stresses

**Table 3** Material properties of mortar for fire protection.

Product name	Refractoriness (SK) <sup>a</sup>	Modulus of rupture (kg/cm <sup>3</sup> )			Chemical composition			Conductivity (W/m.k) <sup>b</sup>
SUPER #3000	33	110 °C	550 °C	1100 °C	Al <sub>2</sub> O <sub>3</sub>	SiO <sub>2</sub>	Fe <sub>2</sub> O <sub>3</sub>	0.41
		93	79	79	52.2	44	0.2	

<sup>a</sup> International standard refractory code for SK.

<sup>b</sup> Test result done by Korea Conformity Laboratories

**Table 4** Material properties of fire board.

Product name	Density (g/cm <sup>3</sup> )	Contraction ratio (%) <sup>a</sup>	Modulus of rupture (N/mm <sup>2</sup> )			Conductivity (W/m k)
Taikalite	0.45	0.39	15 mm	25, 30 mm	45 mm	0.063 <sup>b</sup>
			1.3 or higher	1.7 or higher	2.4 or higher	

<sup>a</sup> Result of a 24-h test at a temperature of 927 °C.

<sup>b</sup> Test result done by Korea Conformity Laboratories.

**Table 5 Bond strength of EB and NSM-FRP.**

Specimen name	$P_u$ (kN)	$\sigma_f$ $P_u/A_f$ (N/mm <sup>2</sup> )	$f_n/f_{fu}$	$\tau_f$ $P_u/A_b$ (N/mm <sup>2</sup> )
E-F0-S0	15.33	375	0.16	4.5
N-F0-S0	22.79	1117	0.48	6.7

\*  $f_n$  is strength of specimen; the peak load was divided by sectional area of FRP.  $f_{fu}$  is the ultimate strength of FRP, 2319 N/mm<sup>2</sup> which was given from tensile test,  $\tau_f$  is bond stress acting between FRP and concrete.

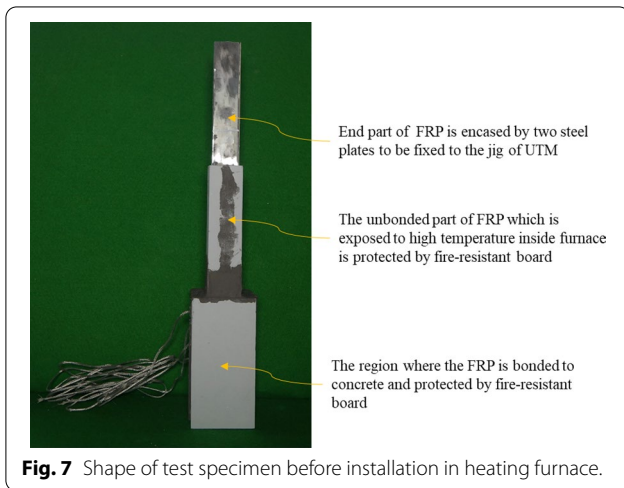


**Fig. 7** Shape of test specimen before installation in heating furnace.

were lost while keeping a stress of 40% of the maximum bond strength of E-F0-S0 or N-F0-S0. Temperatures were measured at the top and middle surfaces of the test specimens and the average of these values was taken to be the furnace temperature. The increase in heating temperature over time was attempted to follow the standard fire temperature curve of KS F 2257 (2014, same as the curve of ISO 834), but due to the limitation of electric heating furnace, it is heated to the maximum performance of the heating furnace and the heating was stopped when bond strength deteriorates. Accordingly, there is a difference in time-heating temperature for each specimen. Figure 9 shows the time-temperature curves inside the furnace for all specimen in this experiment.

**2.4 Test Result**

**2.4.1 Bond Strength of the FRP Bonded to Concrete Under Room Temperature**

Figure 10 shows the result of increasing load test until the bond failure at room temperature of 22–24 °C for E-F0-S0 reinforced with EB-FRP and N-F0-S0 reinforced with NSM-FRP. The stresses were obtained by dividing the load by the cross-sectional area of the FRP. The FRP cross section of the E-F0-S0 specimen is twice that of the N-F0-S0 specimen. The behavior of the two specimens shows a linear relationship between displacement and stress as the load increases, and ultimately both specimens show bond

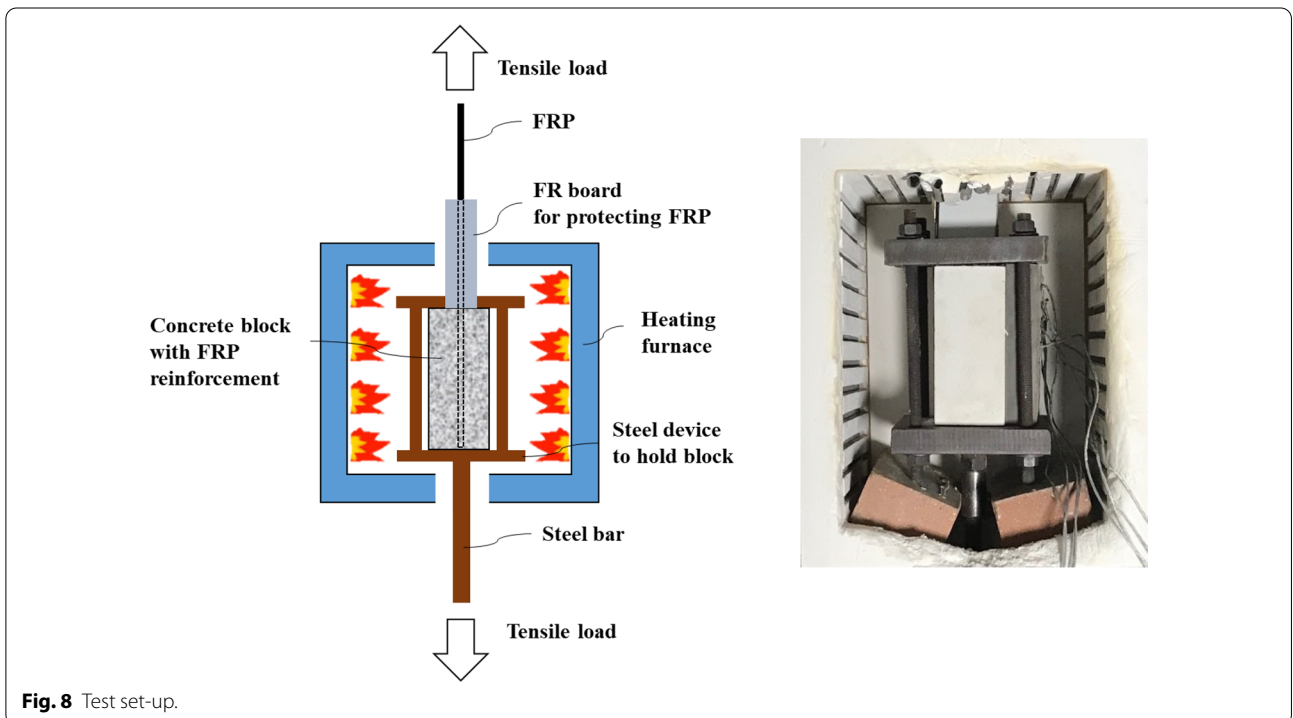


**Fig. 8** Test set-up.

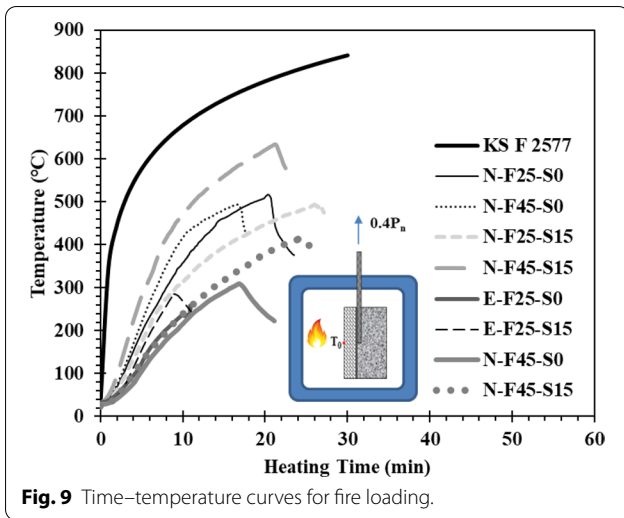


**Fig. 9** Time-temperature curves for fire loading.

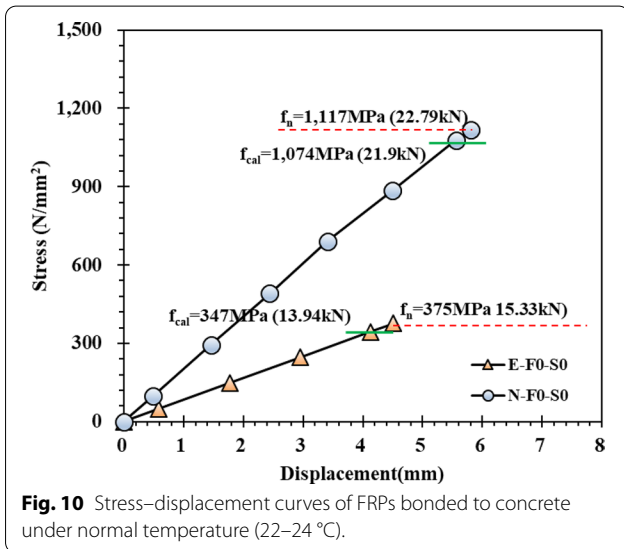


**Fig. 10** Stress-displacement curves of FRPs bonded to concrete under normal temperature (22–24 °C).

failure as intended in the experiment. The maximum tensile forces of E-F0-S0 and N-F0-S0 specimens were 15.33 kN and 22.79 kN, respectively, which are 375 MPa and 1117 MPa in terms of the strength divided by the cross-sectional area. These are 16.17% and 48.17% of FRP's ultimate tensile strength, respectively. If the load is expressed as the shear bond strength divided by the attachment area as shown in Table 5, the values are 4.5 MPa and 6.7 MPa, respectively. It can be seen that the shear bond strength of FRP is higher in NSM than in EB as in the previous studies (Sena Cruz and Barros 2004; Lorenzis et al. 2004; Teng et al. 2006; Seracino et al. 2007; Al-Mahmoud et al. 2012; Seo et al. 2011, 2013, 2016a, b). In this experiment, NSM specimen showed 1.49 times higher shear bond strength

than EB specimen. These shear bond strengths of FRP reinforced with EB or NSM also can be estimated using Eq. (1–4) suggested by Seo et al. (2011, 2013).

$$T_{f1} = \phi b_f t_f f_{yf} \text{ (Tension failure of FRP), [kN]} \quad (1)$$

$$T_{f2} = \lambda \tau_f (2b_f l_d) \text{ (Shear failure of epoxy bond), [kN]} \quad (2)$$

$$T_{f3} = 0.57 \beta \sqrt{f_{ck}} A_{cf} \text{ (Split failure of concrete), [kN]} \quad (3)$$

$$T_f = \min . \{ T_{f1}, T_{f2}, T_{f3} \}, \text{ [kN]} \quad (4)$$

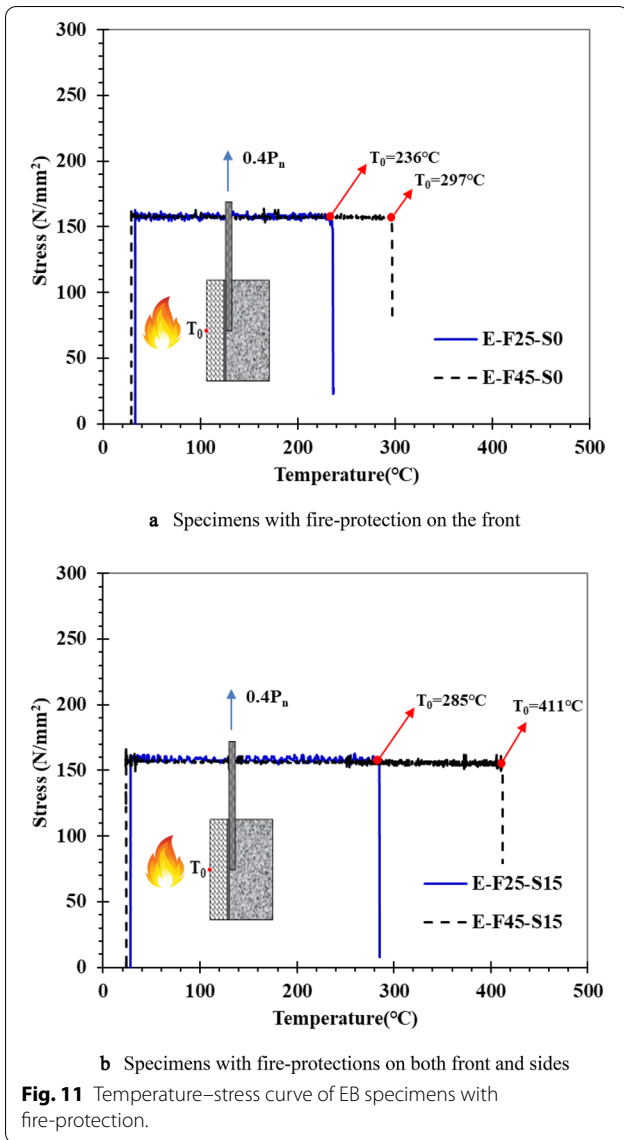
where  $b_f$  and  $t_f$  are width and thickness of FRP, respectively,  $f_{yf}$  is tensile strength of FRP,  $\lambda$  is effective reduction factor of bond,  $\tau_f$  is shear strength of epoxy,  $l_d$  is bond length,  $\beta$  is experimental coefficient,  $A_{cf}$  is surface area of split failure of concrete.

The shear bond strength of EB specimens was governed by Eq. (2) and the value was 13.94 kN while that of NSM specimen was 21.9 kN which was determined by Eq. (3). These values showed good response as 1.1 and 1.04 times of actual experimental results, respectively. From this, it can be seen that the shear bond strength can be properly predicted using these equations.

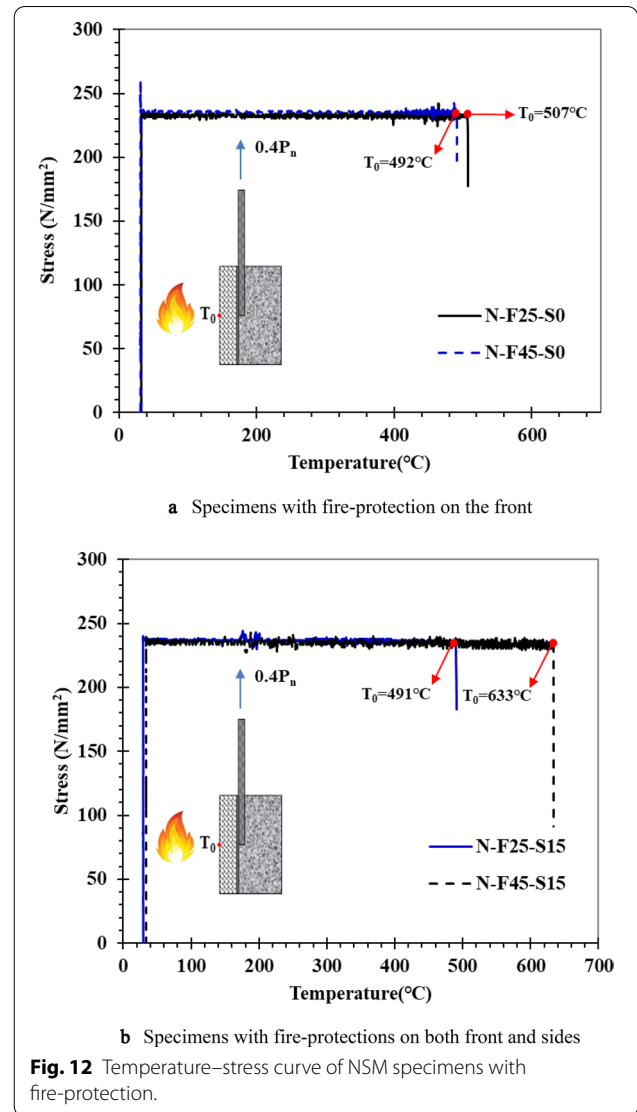
#### 2.4.2 Fire Resistance of EB and NSM-FRPs Bonded to Concrete with the Insulation of FP Mortar and Board

To determine the exposure temperature when a bond failure occurs according to the method of FRP reinforcing to concrete and fire-protection, load corresponding to about 40% of the ultimate bond strength obtained from tensile tests, i.e., 5.98–6.13 kN (155–160 MPa) for EB specimens and 8.92–9.29 kN (232–242 MPa) for NSM specimens, were kept constant after applying.

Figures 11 and 12 represent the graphs showing the change of bond stress with increasing exposure temperature of the specimens with fire-protection after EB and NSM systems, respectively. In EB specimens, the E-F25-S0 and E-F45-S0 specimens insulated with FP boards of 25 mm and 45 mm only on the front face with FRP, respectively, showed bond failure at furnace temperatures of 236 °C and 297 °C, respectively. The E-F25-S15 and E-F45-S15 specimens, which were insulated not only on the front face with FRP but also on both sides with a 15-mm FP board, showed bond failure at furnace temperatures of 285 °C and 411 °C, respectively. From this, it can be seen that as the FP board becomes thicker, the resistance temperature increase, and if the FP board is installed on the both sides as well as the face with FRP, the temperature at which bond failure occurs increases.

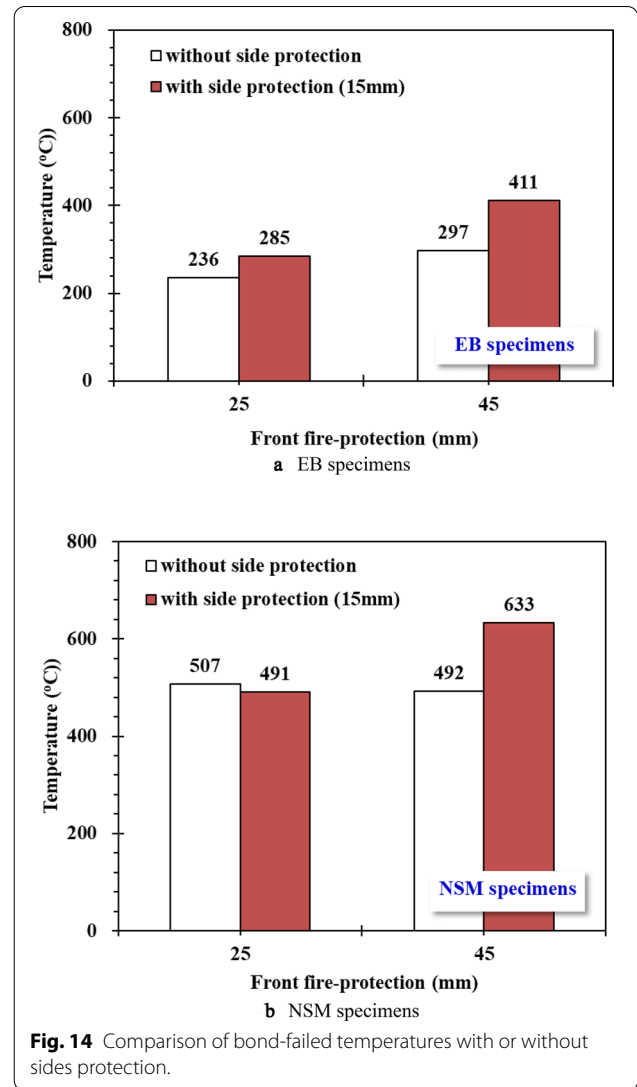
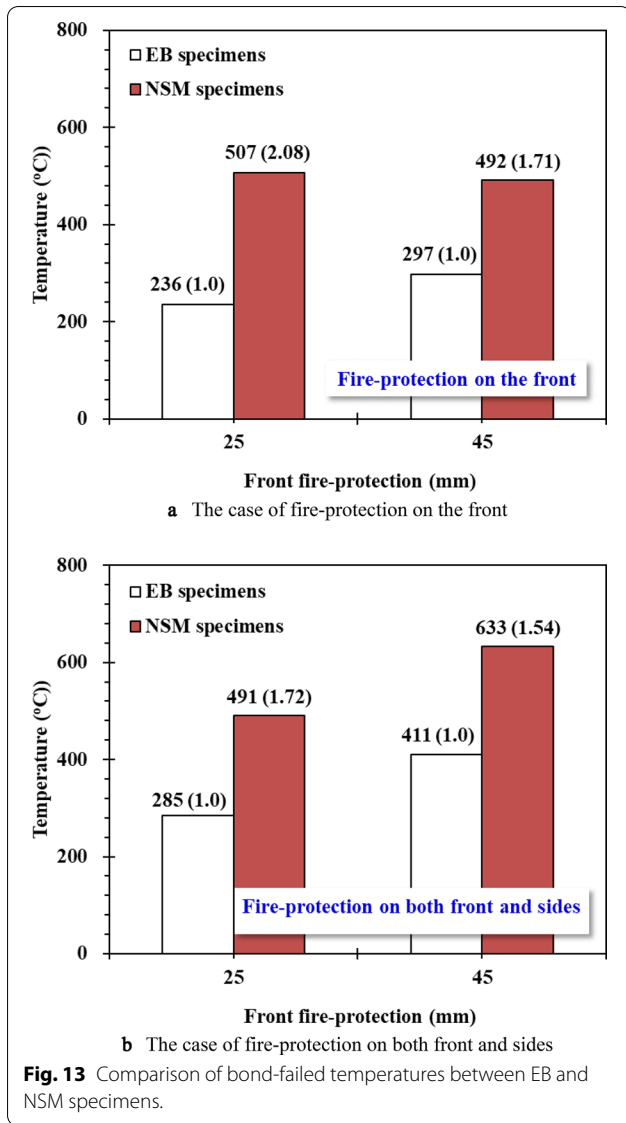


In NSM specimens, N-F25-S0 and N-F45-S0 specimens insulated with 25 mm and 45 mm FP boards only on the front face with FRP, respectively, showed bond failures at furnace temperatures of 507 °C and 492 °C, respectively. N-F25-S15 and N-F45-S15 specimens, which were insulated not only on the front face with FRP but also on both sides with a 15-mm FP board, showed FRP bond failures at 491 °C and 633 °C, respectively. In this result, if there are no side insulation of FP boards, the difference as the thickness of FR board for the face with FRP increases from 25 to 45 mm is not large. This means that if there are no insulation of FP boards on both sides, the epoxy easily reaches its critical temperature by the heat penetrated to the sides, and increasing the thickness of the FP board alone for



the face with FRP does not increase the fire-resistance capacity. On the other hand, if there are insulations with FP boards on the face with FRP and both sides, there is an increase in bond failure temperature as the thickness of the FP board increases from 25 to 45 mm. In other words, the heat transfer is effectively delayed in proportion to the thickness of the FP board on the face with FRP as the heat shield is sufficiently made in the sides.

Figure 13 shows the comparison of bond-failed exposure temperature of EB and NSM specimens with same thickness of FP boards. In case of the specimens with 25-mm and 45-mm FP boards only on the face with FRP, the bond failures of NSM specimens occurred at 2.08 and 1.71 times higher temperatures than the EB specimens, respectively. When the specimens are insulated with



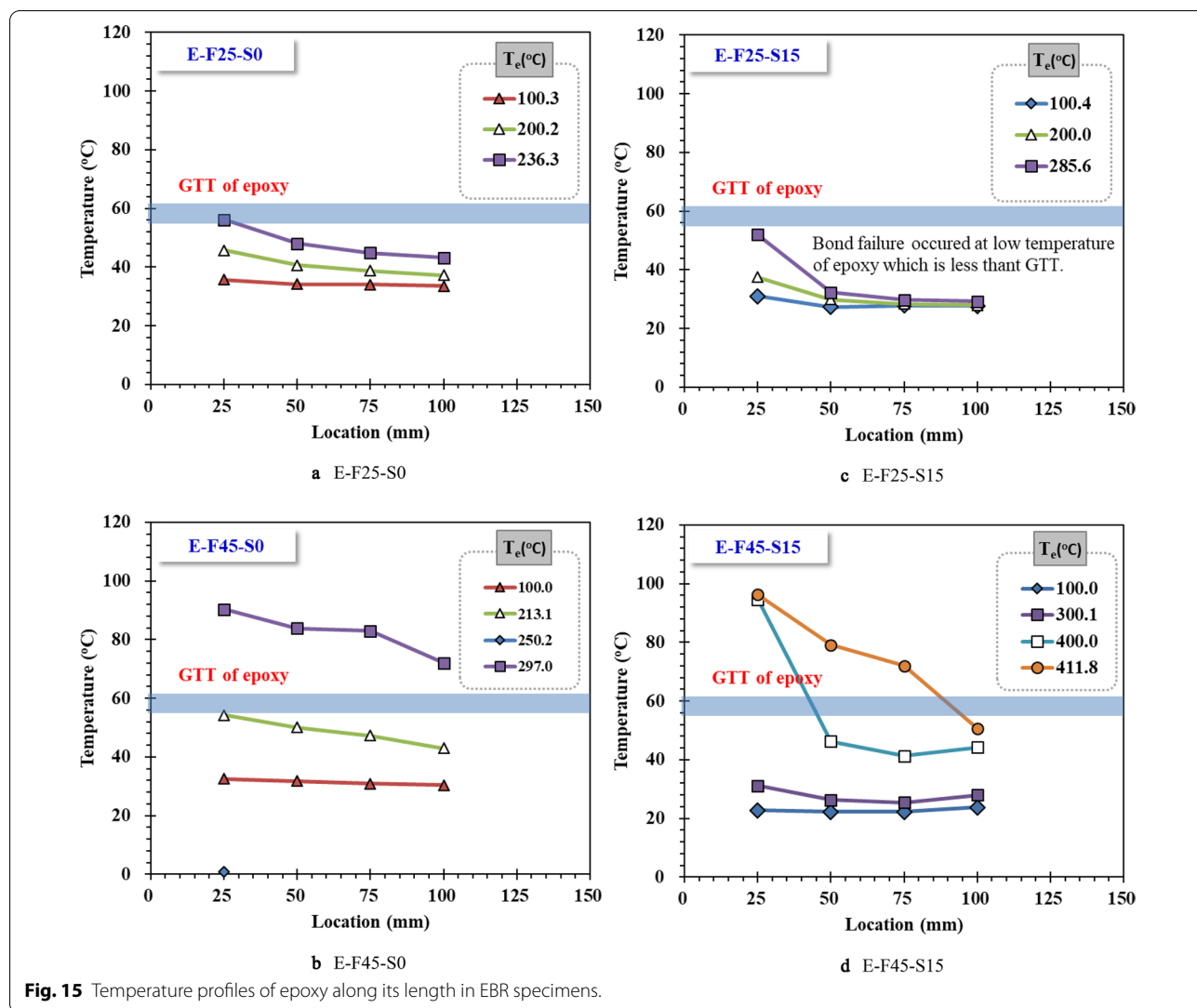
25-mm and 45-mm FP boards on the front face with FRP as well as with 15-mm FP board on both sides, the NSM specimens showed bond failure at the temperature which are 1.72 and 1.54 times higher than the EB specimens, respectively. From this, it can be seen that NSM system have a much higher resistance to high temperatures than EB system with same fire-protection.

Figure 14 shows the difference between the presence and absence of fire-insulation on both sides. In EB specimens, as both sides of the specimen were protected with FP boards, the bond failure temperature at the interface of FRP increased. In NSM specimens, however, the positive effect of the side protection in case of with 25-mm FP board on the front is not appeared. This means that the increase of temperature is controlled by

the heat transferred to the front part. From this, it can be seen that in the case of EB system, even at low temperatures, the heat from the sides is rapidly transferred. On the other hand, in the case of NSM system, the heat transfer from the sides seems to be delayed to a relatively high temperature since the FRP is located inside the groove.

### 2.4.3 Temperature Profiles at Epoxy Inside of Fire-Protection

In order for the FRP reinforced in concrete to exhibit its structural function, the bond strength of epoxy must be secured. However, epoxy is very vulnerable to high temperature and ease to lose its bond capacity when its temperature reached to  $T_g$ . As shown in Fig. 2, the temperature of epoxy was measured at each edge distance from the top surface to find the temperature distribution



**Fig. 15** Temperature profiles of epoxy along its length in EBR specimens.

of epoxy for the entire length of FRP; the upper surface is the direction in which tensile stress acts on the FRP. The temperature distribution of each specimen is shown in Figs. 15 and 16. In the figures,  $T_e$  is the temperature inside the furnace. At low temperatures below 100 °C, the temperature of the epoxy does not fluctuate and the temperature at each location is almost constant. As the applied temperature increases, the temperature near the FRP protruding upper surface rose relatively rapidly. E-F25-S15 specimen showed bond failure in the range of 30–50 °C. This low temperature is due to the impact on the interface between FRP and concrete in the process of setting up the specimen. In the N-F25-S15 specimen, a problem occurred in the thermocouple installed at the 25-mm position, so that some data could not be obtained.

In each specimen, the heating furnace temperature and the epoxy temperature profile when bond failure occurred are shown in Table 6 and Fig. 17. When bond

failure occurred, the E-F25-S15 specimen did not reach the  $T_g$  of epoxy in the entire bonded length, and the E-F25-S0 specimen exceeded the  $T_g$  of epoxy in only a location. This phenomenon can be estimated that there was some damage to the attachment region during the assembly process as described above. For all other specimens, the epoxy temperature at the time of bond failure was above the  $T_g$  of epoxy overall.

Figures 18 and 19 show the temperature change of the epoxy at each location of thermocouples for EB and NSM specimens, respectively. It can be seen that the temperature increase at the epoxy is delayed when the FP board is thickened or both sides are protected with FP mortar and board. And this pattern was almost the same regardless of the measurement position. Figure 20 shows the comparison of the temperature profiles of the EB and NSM specimens, located at 100 mm from the edge with the same fire-protection; in this position, the influence of

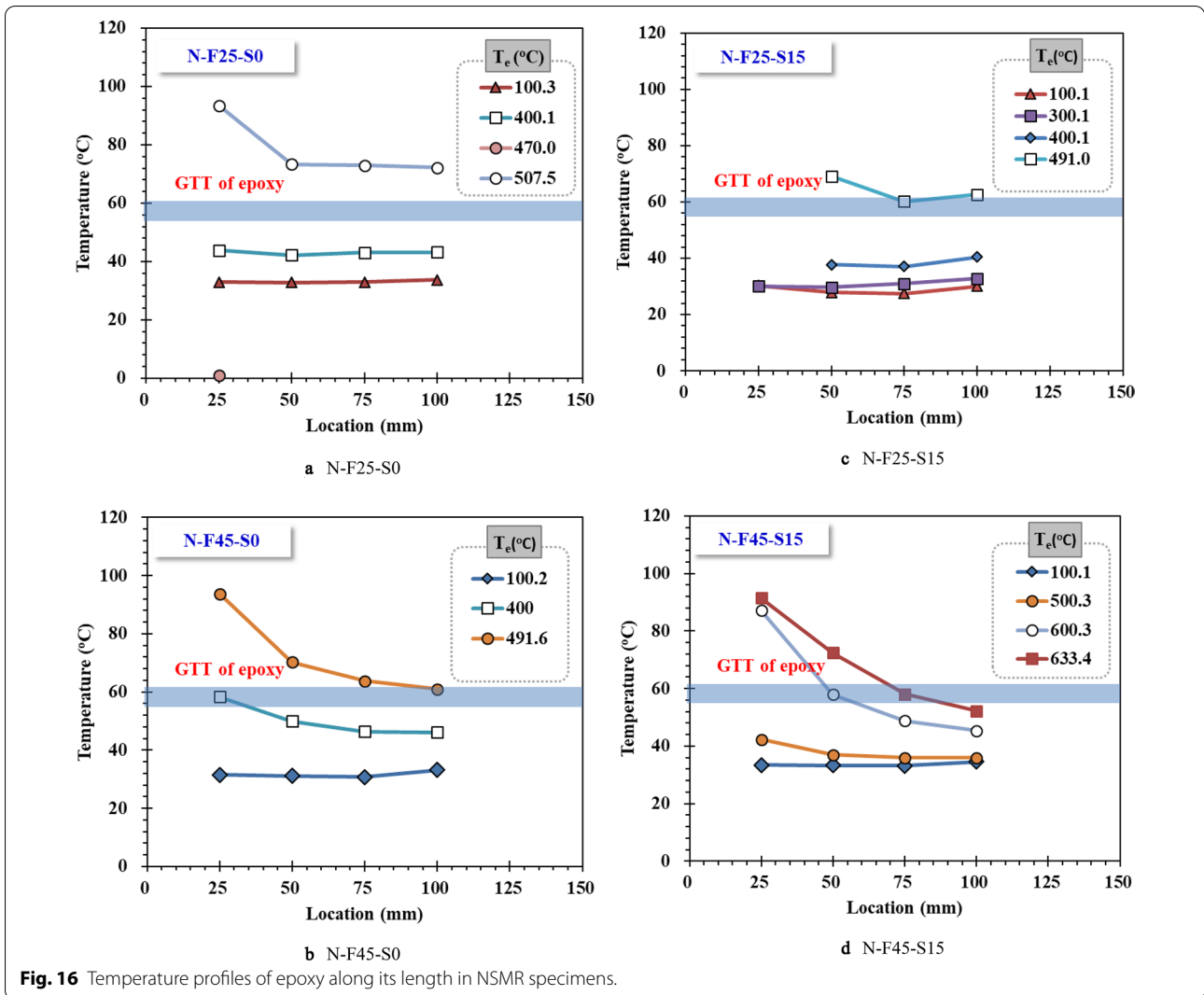
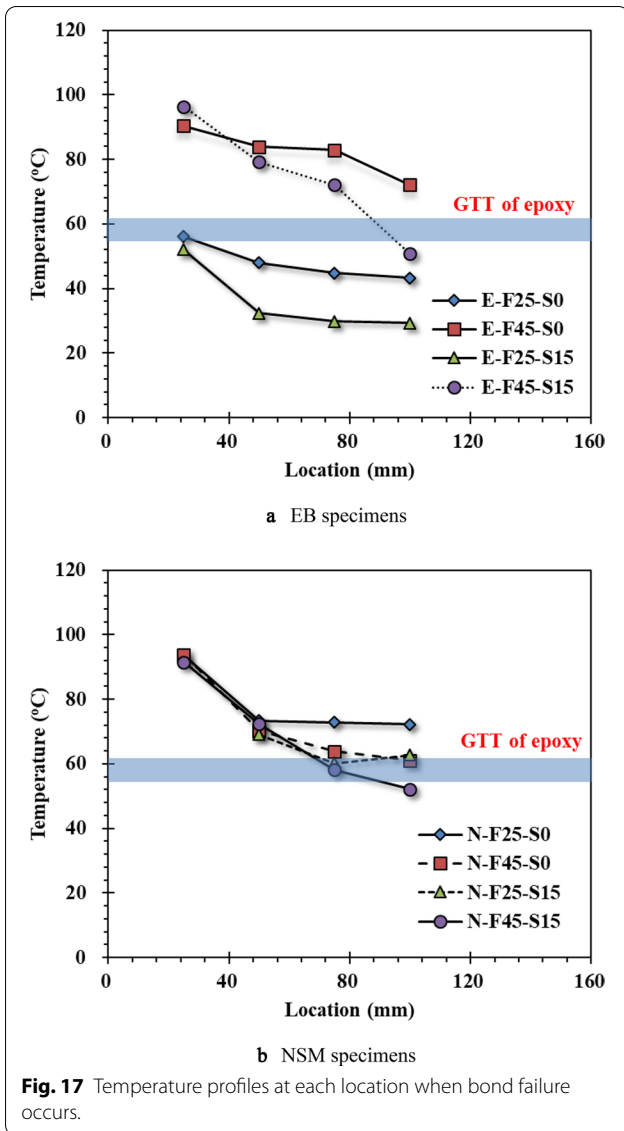


Fig. 16 Temperature profiles of epoxy along its length in NSMR specimens.

Table 6 Temperatures of thermocouples around epoxy when bond failure of FRP occurs.

Specimen Name	Temperature at each location (°C)					Average
	$T_e^a$	$T_{25}$	$T_{50}$	$T_{75}$	$T_{100}$	
E-F25-S0	236.3	56.1	48.0	44.8	43.2	48.0
E-F45-S0	297.0	90.3	83.9	82.9	72.1	82.3
E-F25-S15	285.6	52.0	32.3	29.8	29.3	35.9
E-F45-S15	411.8	96.3	79.2	72.1	50.7	74.6
N-F25-S0	507.5	93.5	73.4	72.9	72.2	78.0
N-F45-S0	491.6	93.8	70.2	63.8	61.0	72.2
N-F25-S15	491.0	-	69.1	60.2	62.7	64.0
N-F45-S15	633.4	91.5	72.4	58.1	52.2	68.6

<sup>a</sup>  $T_e$  is the temperature inside the furnace when the bond failure occurred.

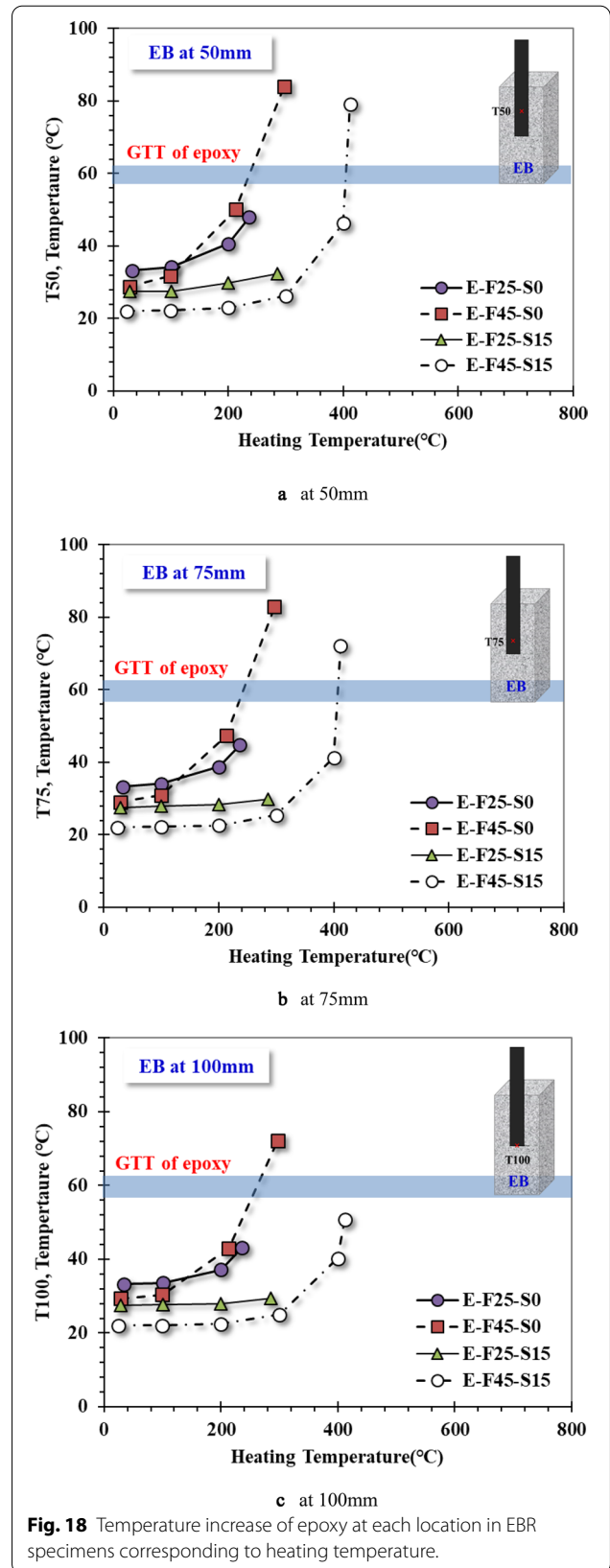


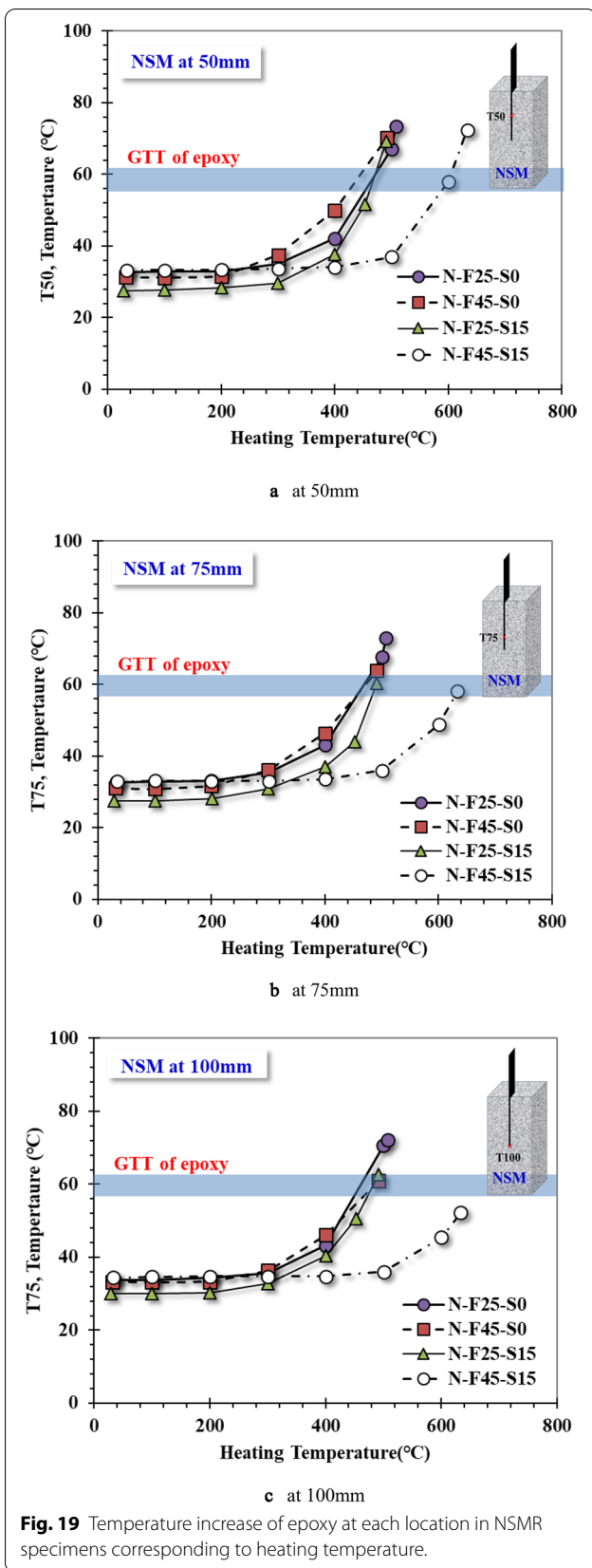
the longitudinal edge distance is minimal. In spite of the same fire-protection, the temperature increase of epoxy in NSM system is delayed compared to that of EB system. The same pattern was observed for the 50-mm and 75-mm positions. Due to this effect, the adhesion damage of the epoxy is delayed, so that NSM system has a higher resistance than EB system in high temperature.

### 3 Prediction of Temperature Transfer to FRP Through FE Analysis

#### 3.1 FE Modeling

To predict the temperature transition to FRP–epoxy interface from outside according to the method of FRP reinforcing and the fire-protection method for the FRP





exposed to high temperature, FE analysis was performed using the MIDAS-FEA program (2010) which was developed for commercial purpose. In this program, the heat conduction equations are analyzed based on conduction in solid materials, and convection is considered as a boundary condition or a form of load. The analyses on the specimens were performed according to the basic thermal conductivity correlation defined in the program. Regarding the thermal conductivity characteristics of FP mortar and board, the results of previous test were considered. In modeling of concrete and FRP, the thermal properties of those suggested by existing researchers were used. The constitute equations for heat transition considered in this program are as follows.

The rate of thermal increase in volume  $V$  can be calculated as Eq. (5) by specific heat and density.

$$\text{Rate of inrease of heat in } V = \int_V \rho c \frac{\partial T}{\partial t} dV, \quad (5)$$

where  $c$  is specific heat ( $J/kg \cdot ^\circ C$ ),  $\rho$  is density ( $kg/m^3$ ).

The heat flow rate transferred by conduction is calculated using temperature gradient and thermal conductivity according to Fourier's law.

$$\text{Rate of heat conduction across } S = \int_S k(\nabla T) \cdot n ds, \quad (6)$$

where  $k$  is thermal conductivity ( $J/m \cdot hr \cdot ^\circ C$ ),  $\nabla T$  is temperature gradient ( $^\circ C/m$ ).

Assuming that the heat generation rate per unit volume is  $Q$  and the thermal conductivity is constant in space and is the same in each direction, Eq. (7) can be obtained from Eqs. (5) and (6).

$$\rho c \frac{\partial T}{\partial t} = k \nabla^2 T + Q. \quad (7)$$

If the above equation is space discretized by the finite element method, it becomes the matrix differential equation for time as Eq. (8), and the analysis result is the node temperature for each time.

$$C \dot{T} + KT = R, \quad (8)$$

where  $C$  is capacitance matrix,  $K$  is conduction matrix,  $R$  is heat load vector.

The heat capacity is calculated by density and specific heat. Thermal conductivity is a matrix of elements calculated by thermal conductivity, and the influence of convective boundary conditions is reflected. The heat load is calculated by heat source, heat flux, heat flow, etc., and the influence of convective boundary conditions is reflected.

Figure 21a, b shows the modeling of EB and NSM specimens, respectively. The element types of FRP, concrete,

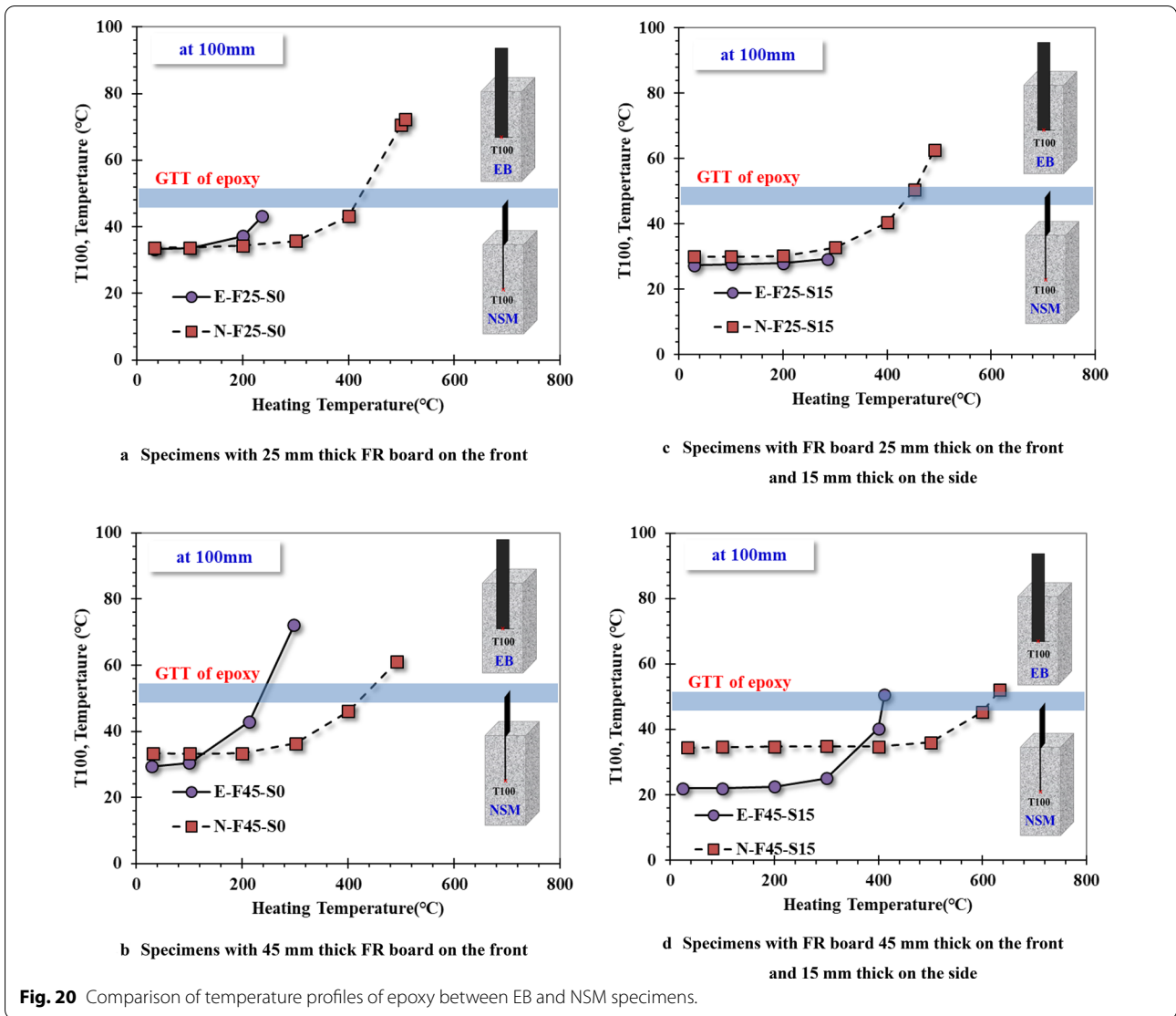


Fig. 20 Comparison of temperature profiles of epoxy between EB and NSM specimens.

and FP board are all solid elements, and the basic mesh size of concrete is a cube having a width of 10 mm. FRP was modeled with the same mesh size and thickness of only 1.2 mm and 5 mm, respectively. The FP board also has the same mesh size with a thickness of 10 mm or 5 mm. Each contact surface of concrete, FRP, FP-mortar and FB boards was all assumed to be complete adhesion. The specific heat of concrete was considered to change with temperature as defined in Eurocode 2 (2004), Eq. (9). For the thermal conductivity of concrete, the average value of the upper and lower limits set in Eurocode 2 was used as shown in Fig. 22. Equations (10) and (11) represent the upper and lower limit curves of thermal

conductivity of concrete specified in Eurocode 2, respectively. The density and specific heat of FRP, FP mortar and board are shown in Table 7. Epoxy resin was not considered in the modeling because it has very thin thickness and their influence is negligible in the transition analysis.

$$\begin{aligned}
 c_p &= 900 \text{ (J/kg K)}, & \text{for } 20^\circ\text{C} \leq \theta \leq 100^\circ\text{C} \\
 c_p &= 900 + (\theta - 100) \text{ (J/kgK)}, & \text{for } 100^\circ\text{C} \leq \theta \leq 200^\circ\text{C} \\
 c_p &= 1000 + (\theta - 200)/2 \text{ (J/kg K)}, & \text{for } 200^\circ\text{C} \leq \theta \leq 400^\circ\text{C} \\
 c_p &= 1100 \text{ (J/kg K)}, & \text{for } 400^\circ\text{C} \leq \theta \leq 1200^\circ\text{C}
 \end{aligned}
 \tag{9}$$

where  $\theta$  is concrete temperature.

$$\lambda_c = 2 - 0.2451 \left( \frac{\theta}{100} \right) + 0.0707 \left( \frac{\theta}{100} \right)^2 \text{ (W/mK)}, \text{ for } 20^\circ\text{C} \leq \theta \leq 1200^\circ\text{C}
 \tag{10}$$

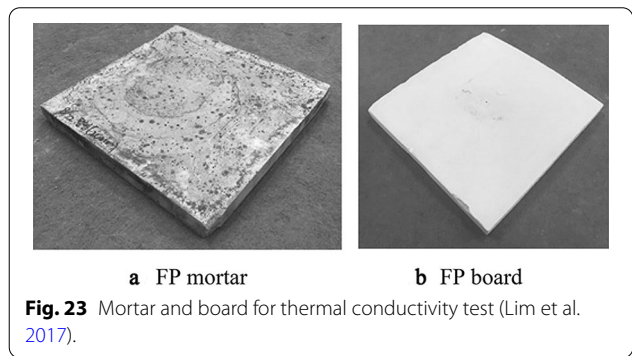
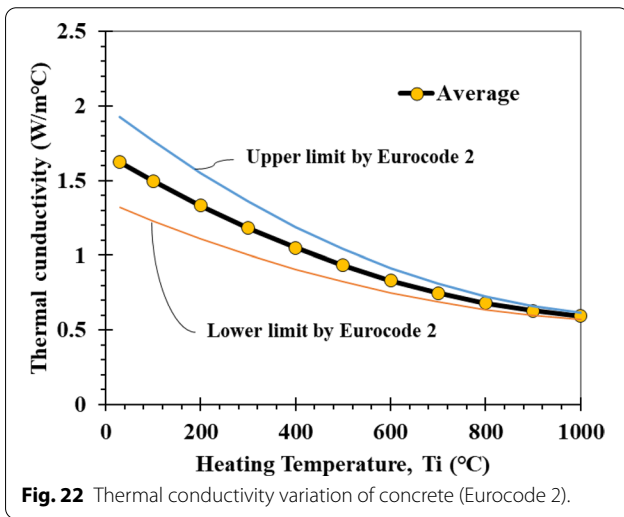
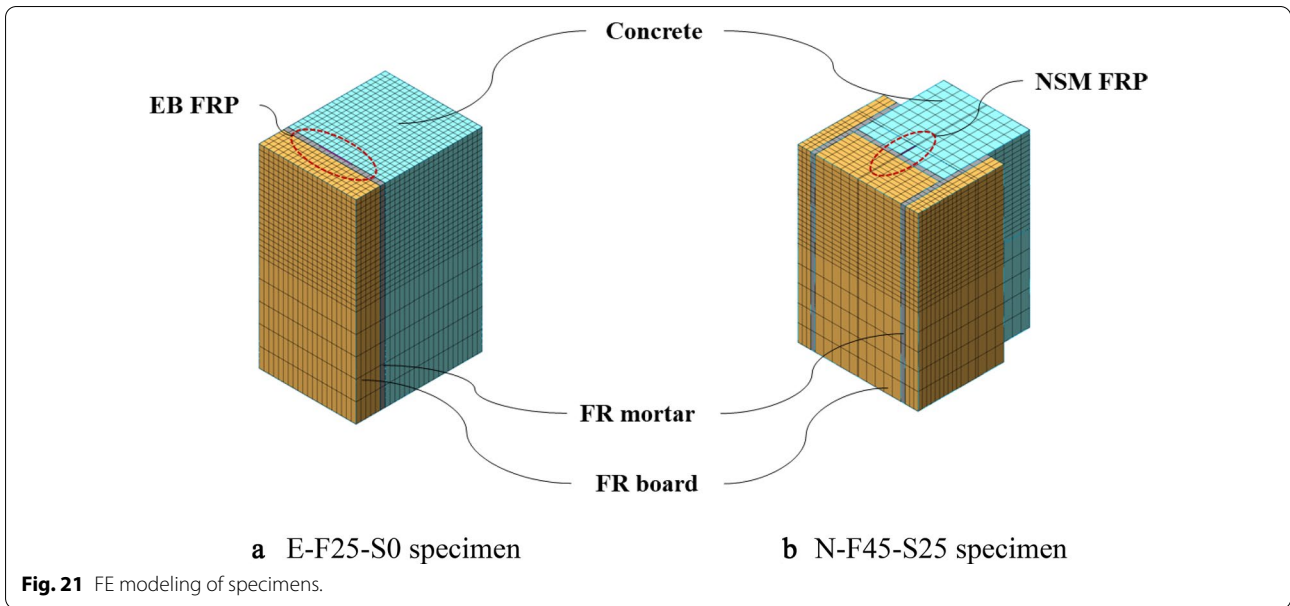


**Table 7 Thermal properties of materials at room temperature for FE analysis.**

Material type	Density (kg/m <sup>3</sup> )	Specific Heat (J/kg °C)
CFRP	1550	848 (270 K), 1485(500 K) <sup>a</sup>
Mortar	2360	837
Board	400	1000

These values were provided by manufacturers.

<sup>a</sup> () is exposed temperature.

In predicting the temperature at the epoxy during high-temperature exposure through FE analysis, it is important to understand the thermal conductivity of fire-protection materials. For this purpose, the thermal conductivity test results of Lim et al. (2017) for FP mortar and board are identical to those used in this study. Figure 23 is pictures of FP mortar and board. In the thermal conductivity test, as shown in Fig. 24, after installing FP mortar or board at the entrance of the furnace, the temperature of the outer surface of the specimen was measured while increasing the internal temperature. Figure 25a, b shows the inside view of the furnace and the installed specimens, respectively. The relationships between the inside and outside

$$\lambda_c = 1.36 - 0.136 \left( \frac{\theta}{100} \right) + 0.0057 \left( \frac{\theta}{100} \right)^2 \text{ W/mK, for } 20^\circ\text{C} \leq \theta \leq 1200^\circ\text{C.} \tag{11}$$

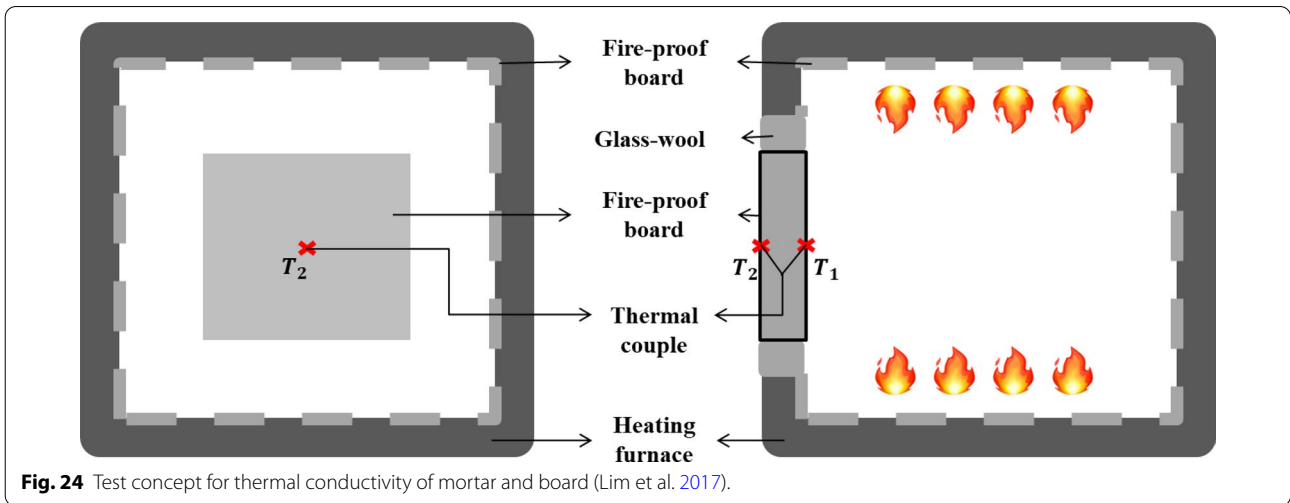


**Fig. 24** Test concept for thermal conductivity of mortar and board (Lim et al. 2017).

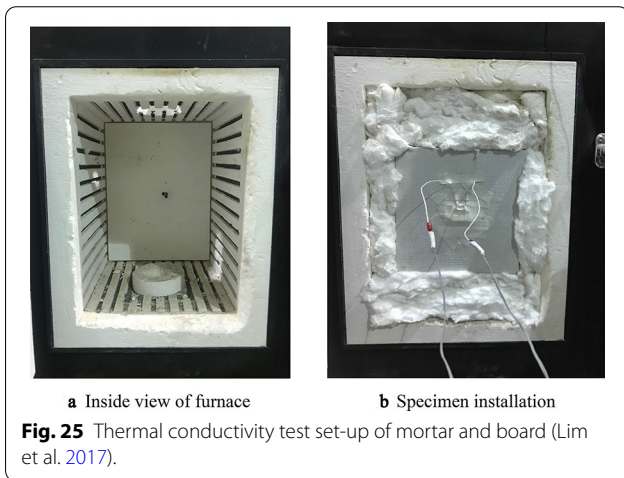


**Fig. 25** Thermal conductivity test set-up of mortar and board (Lim et al. 2017).

temperature observed in the experiment are shown in Fig. 26. To find a proper relationship of the thermal conductivity of these materials with time through FE analysis, the repeated analysis was performed using MIDAS-FEA program. The used density and specific heat of FP mortar and board are as shown in Table 7 which are from the manufacturers. From the repeated analysis under constant specific heat, the thermal conductivity of each material corresponding to the temperature can be expressed as Eqs. (12) and (13) for the FP mortar and board, respectively. As shown in Fig. 26, it is shown that the analysis results using the relationships of the thermal conductivities of FP mortar and FP board are very close to the experimental results.

$$k_m = 0.023e^{0.0033T_i}, \tag{12}$$

$$k_b = 0.0001T_i - 0.0096 > 0.002, \tag{13}$$

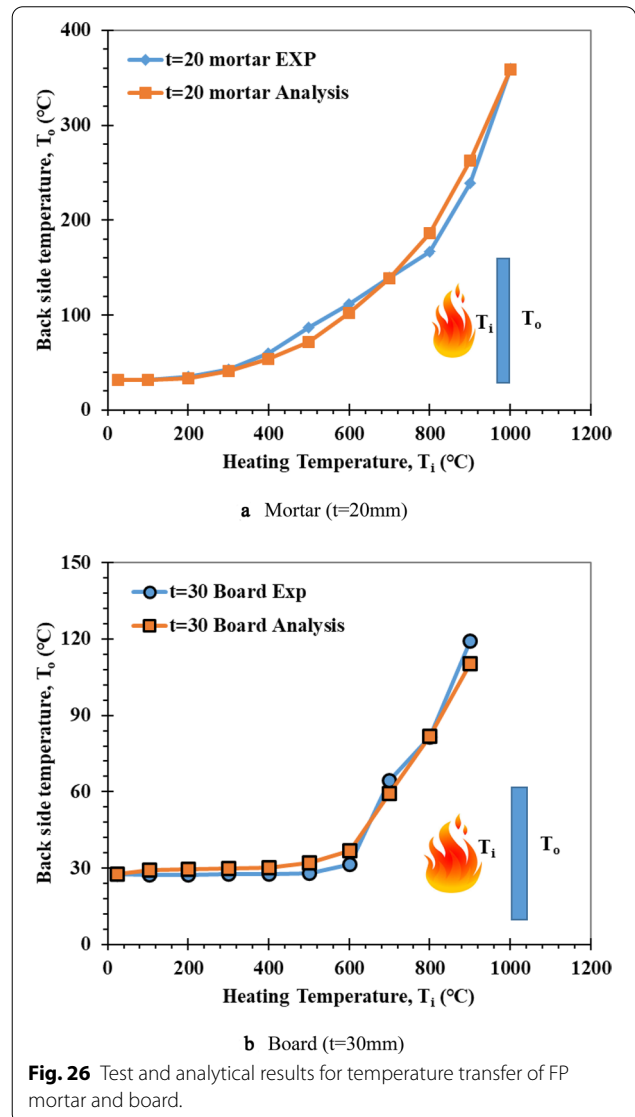


**Fig. 26** Test and analytical results for temperature transfer of FP mortar and board.

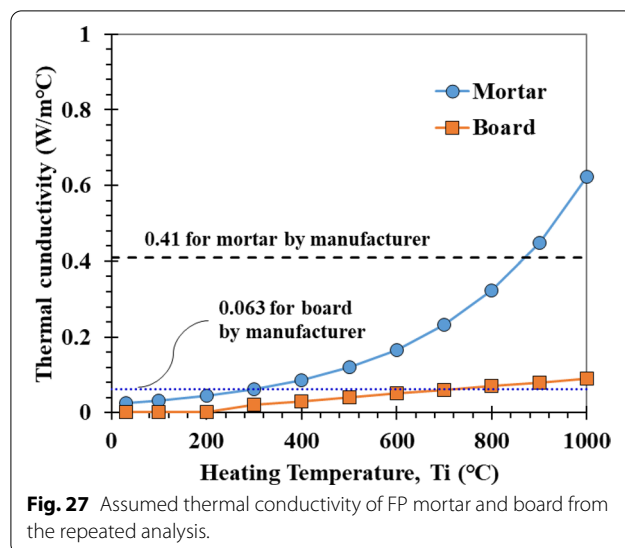
where  $k_m$  and  $k_b$  are the thermal conductivity of FP mortar and board, respectively.  $T_i$  is input temperature.

Accordingly, the values obtained from Eqs. (12) and (13) were used as conductivities of FP mortar and board, respectively, in FE modeling of the block specimens as shown in Fig. 27. Thermal loads were applied to the entire exposed surface in the same way as the actual experimental conditions. However, it was not applied to the unexposed part of the upper surface of the test specimens as shown in Figs. 7 and 8. As described previously, since the time–heating temperature relationship is not the same for each specimen, the increment of the exposure temperature for each specimen followed the time–heating curve relationship considered in each experiment as shown in Fig. 9. In the FE analysis, the convection condition of the surface of the specimen inside the furnace was considered as free convection. Regarding the coefficient value for the convective heat transfer coefficient in air, 2.5–25 W/m<sup>2</sup> K is used in free condition (Kosky et al. 2013). In this analysis, the temperature load was applied directly to the surface of the specimen using 25 W/m<sup>2</sup> K as the convective heat transfer coefficient. There was no difference in the analysis result due to the change in the convective coefficient in the air. The reason for doing this is that even in actual experiments, the temperature inside the furnace was measured to be uniform throughout.

### 3.2 Analysis Result and Comparison with Test Result

As a result of analysis, Fig. 28 shows the temperature distribution at 50 mm from the edge at the maximum exposure temperature of each specimen. In all specimens, the location where FRP is located has the lowest temperature. In addition, the temperature increase is relatively high at the corners where heat is transferred in the vertical and horizontal directions. In the case of the surface with the fire protection, the temperature is low due to the effect of the insulation. The maximum exposure temperature considered in the analysis is the maximum temperature acted upon in the actual experiment, and the temperature of the epoxy at that time is shown in the figure. The temperature distributions at 75 mm and 100 mm showed almost similar distributions.

Figure 29 shows the temperature of epoxy at 100 mm from the edge of each specimen, compared with the experimental results; 100 mm is the position where the edge effect is the least. In the N-F25-S0 and N-F45-S0 specimens without both side protections, the temperature obtained from the analysis is higher than the temperature observed in the experiment as a whole. The reason for this is that there was an effect of delaying heat

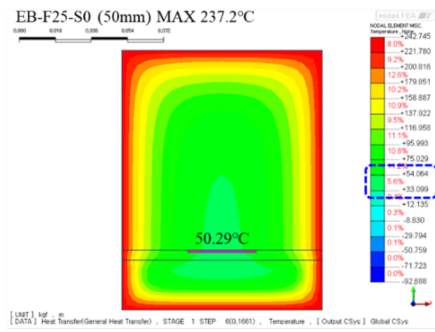


transfer from the side surfaces by the FP mortar in the experiment, but the effect was not properly reflected in the analysis. In the temperature distribution of Fig. 28, when the E-F25-S0 and E-F45-S0 specimens are failed in bond, the temperature of the side below is lower than that of the upper part. On the other hand, the temperature distributions at sides of N-F25-S0 and N-F45-S0 specimens, which were bond-failed at relatively high temperatures, showed no such difference. In other words, the effect of FP mortar is reflected at a temperature of less than 300 °C but not properly reflected at higher temperatures. In other specimens, the analytically predicted temperatures were similar to those observed in the experiment.

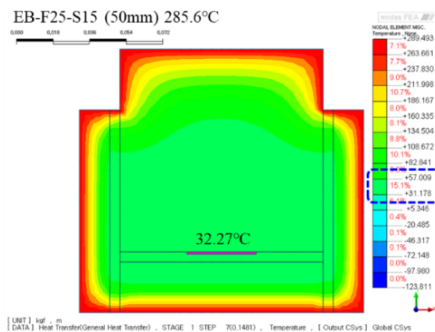
In the fire-protection of the actual structure, it is desirable to protect the heat transfer from the face with FRP as well as from both sides. Therefore, if the fire-protection at sides is conducted in this way, it is considered that the expected temperature of epoxy after the fire-protection can be predicted properly when the FE analysis is performed according to the method considered in this study.

### 4 Conclusions

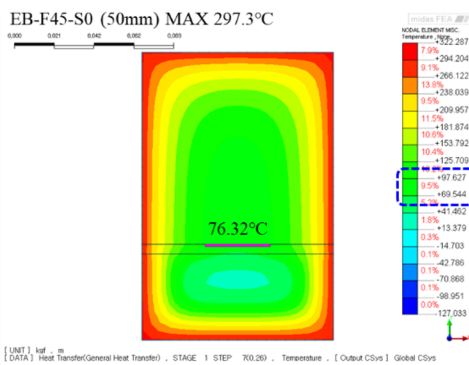
In this study, the fire-resistance performances of the EB and NSM-FRP systems with the insulation of board and mortar were evaluated by high-temperature exposure tests. In particular, by gradually increasing the exposure temperature in a state where a constant tensile stress is applied to the FRP reinforced to concrete, the temperature at which the bond strength of the FRP is lost is determined according to the fire-insulation detail. In addition, a finite element analysis was performed to predict the temperature of the epoxy by increasing the



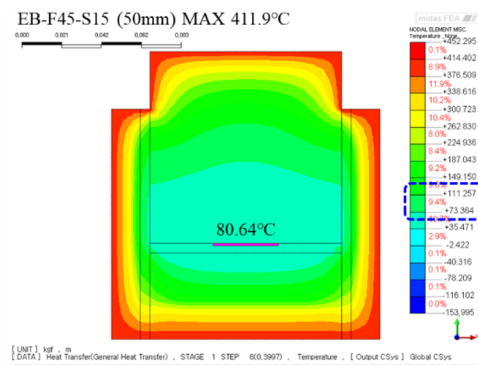
a E-F25-S0



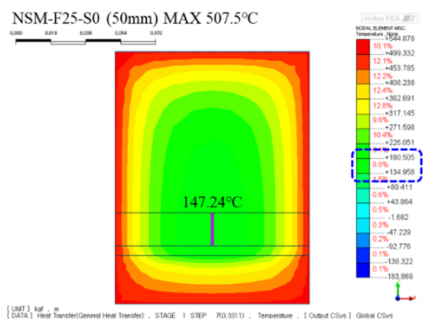
b E-F25-S15



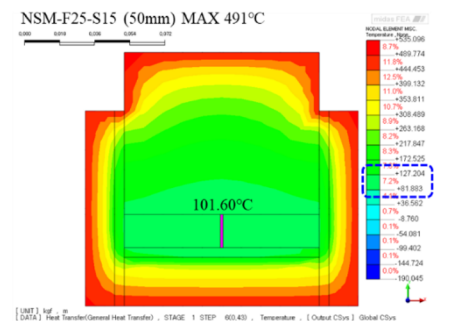
c E-F45-S0



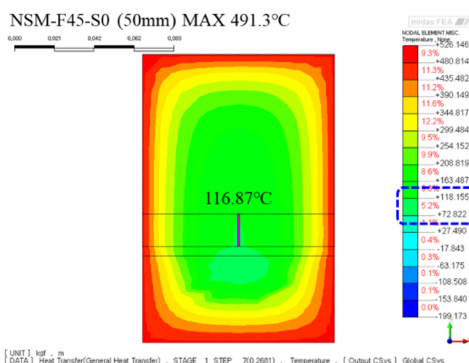
d E-F45-S15



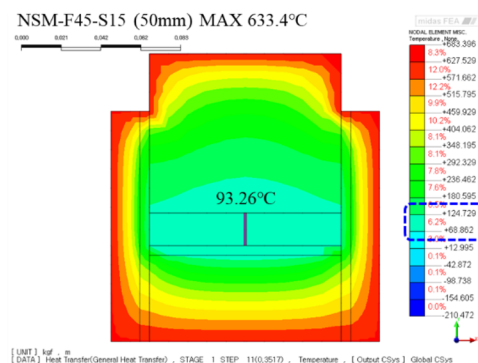
e N-F25-S0



f N-F25-S15



g N-F45-S0



h N-F45-S15

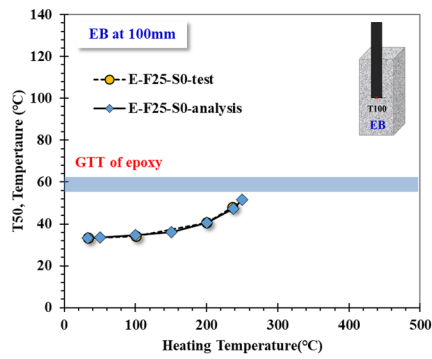
**Fig. 28** Temperature distribution plot at 50mm from the edge when bond failure occurs.

external exposure temperature after fire-insulation and the results were compared with the experimental results. The following conclusions were drawn from the study.

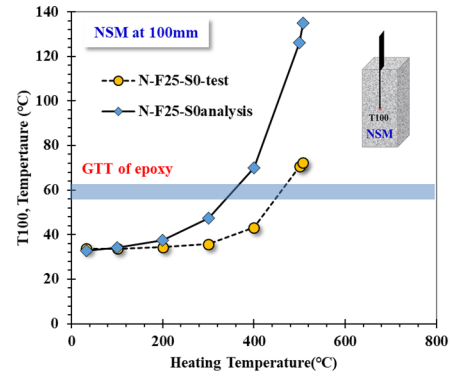
1. As a result of the tensile tests of E-F0-S0 specimen reinforced with EB-FRP and N-F0-S0 specimen reinforced with NSM-FRP at room temperature, the bond strength of NSM specimen was 1.49 times higher than that of EB specimen even with the same adhesion area. In addition, as a result of evaluating the shear bond strength of those using the equations proposed by Seo et al. (2011, 2013), the maximum strength of EB specimens was determined by epoxy bond shear failure, and NSM specimens were determined by concrete-splitting-failure. The predicted maximum strengths of EB and NSM specimens were good response as 1.1 and 1.04 times of actual experimental results, respectively. From this, it is shown that the bond strength of EB and NSM system with strip can be properly estimated using the existing equations.
2. Double shear specimens were made and tested to check the critical temperature of epoxy at which the bond strength of epoxy used for the bonding of FRP disappears. It will ascertain the critical temperature at which the bond strength of the epoxy is lost by causing certain level of shear stress to the epoxy and then exposing it to gradually increasing temperatures. The shear stress acting on the bonded surface of epoxy was lost when the epoxy temperature reaches about 60 °C (54.4–60.5 °C) which is similar to glass transition temperature ( $T_g$ ), 54.5 °C obtained from DSC test. From this,  $T_g$  is close to the critical temperature losing bond strength and it can be obtained by the double shear experiment.
3. To understand the exposure temperature when the adhesion failure occurs according to the method for FRP reinforcing to concrete and fire-protection, a load corresponding to about 40% of its maximum bond strength is maintained at normal temperature (22–24 °C) and then exposed to high temperature. As a result of the test, despite the same fire-protection, NSM specimens were able to resist 1.54–2.08 times higher temperature than EB specimens.
4. Increasing the thickness of the FP board lowers the temperature increase of the epoxy, but when the heat transfer to the sides is not blocked, the effect is not increased proportionally. In EB specimens which are bond-failed at relatively low temperatures, it was found that there was an increased heat blocking effect as the thickness of the FP board on the face with FRP increased from 25 to 45 mm. On the other hand, NSM specimens exposed to relatively high temperatures did not show an effect of increasing the thickness of FP board from 25 to 45 mm. In the case of fire-protection on both sides as well as the face with FRP, the effect of fire protection increased in both EB and NSM specimens as the thickness of the FP board on the surface with FRP increased. From this, it is necessary to consider the heat transfer from the sides according to the edge distance as well as the heat transferred to the face with FRP for effective fire-protection.
5. Thermal conductance tests and the FE analyses of FP mortar and board were performed to find proper models for thermal conductivity of the materials that varied with temperature. And using the models, the thermal conduction analyses of EB and NSM-FRP with the fire-protection were carried out. As a result of the analysis, the case of the fire protection of both sides as well as the face with FRP showed good correlation between the analysis and test results. However, if there is no fire protection on the sides, it is possible that the analysis temperature is rather high than actual at high temperature, so further research is needed about this matter.
6. For the design purpose of fire-protection about FRP system using FP mortar and board, further analyses considering various conditions are necessary and will be continued in subsequent research.

(See figure on next page.)

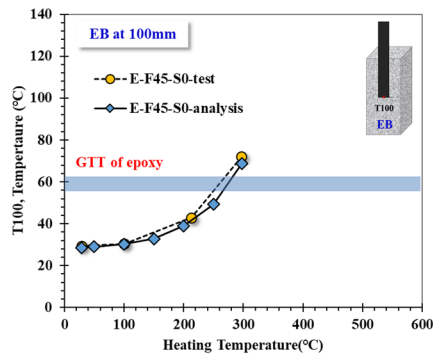
**Fig. 29** Comparison of temperatures at 100mm from the edge between test and analytical result.



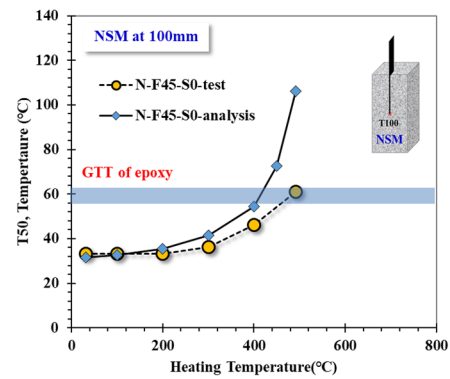
a E-F25-S0



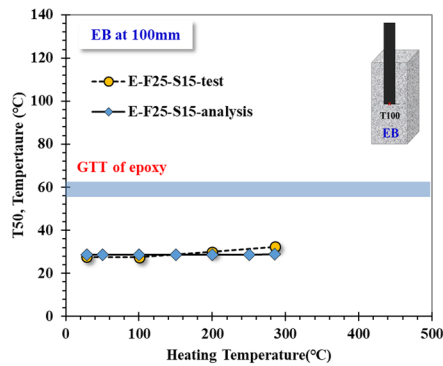
e N-F25-S0



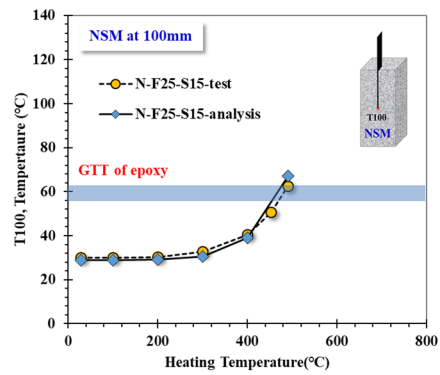
b E-F45-S0



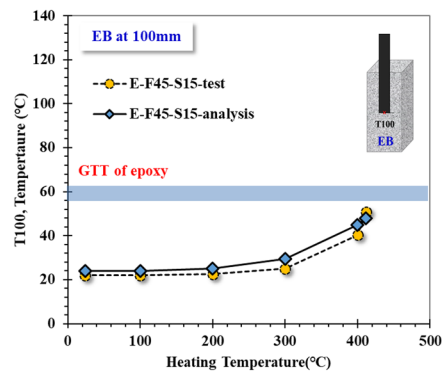
f N-F45-S0



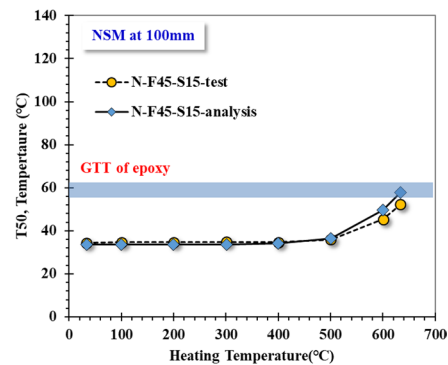
c E-F25-S15



g N-F25-S15



d E-F45-S15



h N-F45-S15

### Acknowledgements

This work was supported by the Korea Agency for Infrastructure Technology Advancement (KAIA) grant funded by the Ministry of Land, Infrastructure and Transport (Grant 19CTAP-C130221-03) and by the National Research Foundation of Korea (NRF) grant funded by the Korea government (MSIT) (No. (2018R1A4A 1025953)).

### Authors' contributions

All authors contributed equally to this paper. Especially, SS made substantial contributions to the conceptualization of the study, analysis of the result, editing and revising the article. JL performed the experiment and analyzed the test result. SJ evaluated the thermal capacity by performing FE analysis. All authors read and approved the final manuscript.

**Authors' information** Soo-yeon Seo is a professor in school of Architecture at Korea National University of Transportation.

Jong-wook Lim is working in Dawon structural engineering Co., LTD. as a structural engineer.

Su-hyun Jeong is a graduate student in school of Architecture at Korea National University of Transportation.

### Availability of data and materials

The experimental data used to support the observations of this study are included in the article.

### Competing interests

The authors declare that they have no competing interests.

### Author details

<sup>1</sup> School of Architecture, Korea National University of Transportation, Chungju, South Korea. <sup>2</sup> Dawon Structural Engineering Co., LTD., Seoul, South Korea.

Received: 6 February 2020 Accepted: 12 November 2020

Published online: 27 January 2021

### References

- ACI Committee 440. (2008). Guide for the design and construction of externally bonded FRP systems for strengthening concrete structures (ACI 440.2R). American Concrete Institute, Farmington Hills, (MI, USA), 2008, 12–13, 22–23.
- ACI Committee 440. (2015). Guide for the design and construction of structural concrete reinforced with fiber-reinforced polymer (FRP) bars (ACI 440.1R-15). American Concrete Institute, Farmington Hills, (MI, USA), 2015, 12–13, 22–23.
- ASTM E119. (2007). Standard Test Methods for Fire Tests of Building Construction and Materials
- Ahmed, A. and Kodur, V. K. R. (2010). Performance of FRP-strengthened reinforced concrete beams under design fire exposure. *Proceedings of the Sixth International Conference-Structures in Fire*, Michigan State University
- Al-Mahmoud, F., Castel, A., & Francois, R. (2012). Failure modes and failure mechanisms of RC members strengthened by NSM CFRP composites—Analysis of pull-out failure mode. *Composites Part B: Engineering*, 43(4), 1893–1901.
- Bisby, L. A., Green, M. F., & Kodur, V. K. R. (2005). Fire endurance of fiber-reinforced polymer-confined concrete columns. *ACI Structural Journal*, 102(6), 883–891.
- Blontrock, H., Taerwe, L., & Matthys, S. (1999). Properties of fibre reinforced plastics at elevated temperatures with regard to fire resistance of reinforced concrete members. *ACI Structural Journal*, 188(5), 43–54.
- Blontrock, H., Taerwe, L., and Vandeveld, P. (2001). Fire testing of concrete slabs strengthened with fibre composite laminates. Proc., FRPRCS-5, C. Burgoyne, ed, Thomas Telford Publishing, London, 547–556.
- Burke, P. J., Bisby, L. A., & Green, M. F. (2013). Effect of elevated temperature on near surface mounted and externally bonded FRP strengthening systems for concrete. *Cement and Concrete Composites*, 35(1), 190–199.
- Chowdhury, E. U., Bisby, L. A., Green, M. F., & Kodur, V. K. R. (2008). Residual behaviour of fire-exposed reinforced concrete beams prestrengthened in flexure with fiber-reinforced polymer sheets. *Journal of Composites for Construction*, 12(1), 61–68.
- Dai, J., Gao, W., & Teng, J. (2015). Finite element modeling of insulated FRP-strengthened RC beams exposed to fire. *Journal of Composite Construction*, 19, 1–15.
- European Committee for Standardization. (2004). EN 1992-1-2 design of concrete structures, Part 1–2: General rules-structural fire design, Eurocode 2.
- Fib TG9.3. (2001). *Externally Bonded FRP Reinforcement for RC Structures*. Technical report on the design and use of externally Bonded Fibre reinforced Polymer Reinforcement (FRP EBR) for reinforced Concrete Structures. International Federation for Structural Concrete.
- Firno, J. P., Arruda, M. R. T., & Correia, J. R. (2015). Numerical simulation of the fire behaviour of thermally insulated reinforced concrete beams strengthened with EBR-CFRP strips. *Composite Structures*, 126, 360–370.
- Firno, J. P., Arruda, M. R. T., Correia, J. R., & Rosa, I. C. (2018). Three-dimensional finite element modelling of the fire behaviour of insulated RC beams strengthened with EBR and NSM CFRP strips. *Composite Structures*, 183, 124–136.
- Foster, S. K., & Bisby, L. A. (2008). Fire survivability of externally bonded FRP strengthening systems. *Journal of Composites for Construction*, 12(5), 553–561.
- Hajiloo, H., Green, M. F., Noël, M., Bénichou, N., & Sultan, M. (2017). Fire tests on full-scale FRP reinforced concrete slabs. *Composite Structures*, 179, 705–719.
- Hollaway, L.C. (2011). Key issues in the use of fibre reinforced polymer (FRP) composites in the rehabilitation and retrofitting of concrete structures, Service Life Estimation and Extension of Civil Engineering Structures, 3–74.
- Jiangtao, Y., Yichao, W., Kexu, H., Kequan, Y., & Jianzhuang, X. (2017). The performance of near-surface mounted CFRP strengthened RC beam in fire. *Fire Safety Journal*, 90, 86–94.
- Katz, A., Berman, N., & Bank, L. (1999). Effect of high temperature on bond strength of FRP rebars. *Journal of Composites for Construction*, 3(2), 73–81.
- Kodur, V., & Ahmed, A. (2010). Numerical model for tracing the response of FRP-strengthened RC beams exposed to fire. *Journal of Composites for Construction*, 14(6), 730–742.
- Kodur, V. K. R., & Bhat, P. P. (2018). A numerical approach for modeling response of fiber reinforced polymer strengthened concrete slabs exposed to fire. *Composite Structures*, 187, 226–240.
- Kodur, V. K. R., & Yu, B. (2013). Evaluating the fire response of concrete beams strengthened with near-surface-mounted FRP reinforcement. *Journal of Compos Construction*, 17, 517–529.
- Kodur, V., Bisby, L., & Green, M. F. (2007). Preliminary guidance for the design of FRP-strengthened concrete members exposed to fire. *Journal of Fire Protection Engineering*, 17(1), 5–16.
- Kosky, P., Balmer, R., Keat, W., and Wise, G. (2013). Exploring Engineering, Chapter 12-Mechanical Engineering
- KS F 2257. (2014). Methods of fire resistance test for elements of building construction general requirements. Korea Standards Association.
- Lim, J., Seo, S., & Park, J. (2017). Heat conduction analysis and fire resistance capacity evaluation of reinforced concrete beams strengthened by FRP. *Journal of the Korea Institute for Structural Maintenance and Inspection*, 22(6), 1–8 (in Korean).
- Lorenzis, L., Lundgren, K., & Rizzo, A. (2004). Anchorage length of near-surface mounted fiber-reinforced polymer bars for concrete strengthening—Experimental investigation and numerical modeling. *ACI Structural Journal*, 101(2), 269–278.
- MIDAS Information Technology (2010), Midas FEA 2.0.0
- Nigro, E., Cefarelli, G., Bilotta, A., Manfredi, G., & Cosenza, E. (2011a). Fire resistance of concrete slabs reinforced with FRP bars. Part I: Experimental investigations on the mechanical behavior. *Composite Part B: Engineering*, 42(6), 1739–1750.
- Nigro, E., Cefarelli, G., Bilotta, A., Manfredi, G., & Cosenza, E. (2011b). Fire resistance of concrete slabs reinforced with FRP bars. Part II: Experimental results and numerical simulations on the thermal field. *Composite Part B: Engineering*, 42(6), 1751–1763.
- Palmieri, A. (2012). Evaluation and optimization of fire safety of structures strengthened with NSM reinforcement. Ph.D. thesis, Ghent Univ., Ghent, Belgium.
- Palmieri, A., Matthys, S. and Taerwe, L. (2011). Bond behavior of NSM FRP bars at elevated temperatures, *Proceeding of First Middle East Conference on*

- Smart Monitoring, Assessment and Rehabilitation Civil Structures*, (pp. 1–7), EMPA, Dunai UAE.
- Palmieri, A., Matthys, S., & Taerwe, L. (2013). Fire endurance and residual strength of insulated concrete beams strengthened with near-surface mounted reinforcement. *Journal of Composites for Construction*, 17(4), 454–462.
- Sena-Cruz, J., & Barros, J. (2004). Bond between near surface mounted carbon-fiber-reinforced polymer laminate strips and concrete. *Journal of Composites for Construction*, 8(6), 519–527.
- Seo, S., & Kim, J. (2013). Bond capacity of near-surface-mounted CFRP plate to concrete under various temperatures. *Journal of the Korea Institute for Structural Maintenance and Inspection*, 17(4), 75–83 (in Korean).
- Seo, S., Feo, L., & Hui, D. (2013). Bond strength of near-surface-mounted FRP plate for retrofit of concrete structures. *Composite Structures*, 95, 719–727.
- Seo, S., Yoon, S., Kwon, Y., & Choi, K. (2011). Bond behavior between near surface-mounted fiber reinforced polymer plates and concrete in structural strengthening. *Journal of Korea Concrete Institute*, 23(5), 675–82. (in Korean).
- Seo, S., Choi, K., Kwon, Y., & Lee, K. (2016a). Flexural strength of RC beam strengthened by partially de-bonded near-surface-mounted FRP strip. *International Journal of Concrete Structure and Material*, 10(2), 149–165.
- Seo, S., Lee, M. S., & Feo, L. (2016b). Flexural analysis of RC beam strengthened by partially de-bonded NSM FRP strip. *Composite-B*, 101(15), 21–30.
- Seracino, R., Jones, N., Ali, M., Page, M., & Oehlers, D. (2007). Bond strength of near-surface mounted FRP strip-to-concrete joints. *Journal of Composite Construction*, 11(4), 401–409.
- Siddika, A., Mamun, M. A. A., Ferdous, W., & Alyousef, R. (2020). Performances, challenges and opportunities in strengthening reinforced concrete structures by using FRPs—A state-of-the-art review. *Engineering Failure Analysis*, 111, 104480.
- Teng, J.G., Chen, J.F., Smith, S.T., Lam, L. (2003). Behaviour and strength of FRP-strengthened RC structures: a state-of-the-art review. *Proceeding of the Institution of Civil Engineers—Structures and Buildings*, 156, 51–62.
- Teng, J. G., Lorenzis, L., Wang, B., Rong, L., Wong, T. N., & Lik, L. (2006). Debonding failures of RC beams strengthened with near surface mounted CFRP strips. *Journal of Composites for Construction*, 10(2), 92–105.
- Wang, Y. C., Wong, P. M. H., & Kodur, V. (2007). An experimental study of the mechanical properties of fibre reinforced polymer (FRP) and steel reinforcing bars at elevated temperatures. *Composite Structures*, 80(1), 131–140.
- Williams, B., Kodur, V. K. R., Green, M. F., & Bisby, L. A. (2008). Fire endurance of fiber-reinforced polymer strengthened concrete T-beams. *ACI Structural Journal*, 105(1), 60–67.

### Publisher's Note

Springer Nature remains neutral with regard to jurisdictional claims in published maps and institutional affiliations.

Submit your manuscript to a SpringerOpen<sup>®</sup> journal and benefit from:

- Convenient online submission
- Rigorous peer review
- Open access: articles freely available online
- High visibility within the field
- Retaining the copyright to your article

---

Submit your next manuscript at ► [springeropen.com](https://www.springeropen.com)

---